



Spatiotemporal variations of the $\delta(\text{O}_2/\text{N}_2)$, CO_2 and $\delta(\text{APO})$ in the troposphere over the Western North Pacific

Shigeyuki Ishidoya¹, Kazuhiro Tsuboi², Yosuke Niwa³, Hidekazu Matsueda², Shohei Murayama¹, Kentaro Ishijima², and Kazuyuki Saito⁴

5 ¹National Institute of Advanced Industrial Science and Technology (AIST), Tsukuba 305-8569, Japan,

²Meteorological Research Institute, Tsukuba, Japan, Tsukuba305-0052, Japan,

³National Institute for Environmental Studies, Tsukuba 305-8506, Japan

⁴Japan Meteorological Agency, Tokyo, Japan, Tokyo 105-8431, Japan

Correspondence to: Shigeyuki Ishidoya (s-ishidoya@aist.go.jp)

10 **Abstract.** We analyzed air samples collected onboard a cargo aircraft C-130 over the western North Pacific from May 2012 to March 2020 for atmospheric $\delta(\text{O}_2/\text{N}_2)$ and CO_2 amount fraction. We corrected for significant artificial fractionation of O_2 and N_2 caused by thermal diffusion during the air sample collection by using the simultaneously-measured $\delta(\text{Ar}/\text{N}_2)$. The observed seasonal cycles of the $\delta(\text{O}_2/\text{N}_2)$ and atmospheric potential oxygen ($\delta(\text{APO})$) varied nearly in opposite phase to that of the CO_2 amount fraction at all latitudes and altitudes. Seasonal amplitudes of $\delta(\text{APO})$ decreased with latitude from 34 to
15 25° N, as well as with increasing altitude from the surface to 6 km by 50–70 %, while those of CO_2 amount fraction decreased by less than 20%. By comparing the observed values with the simulated $\delta(\text{APO})$ and CO_2 amount fraction values generated by an atmospheric transport model, we found that the seasonal $\delta(\text{APO})$ cycle in the middle troposphere was modified significantly by a superposition of the northern and southern hemispheric seasonal cycles due to the inter-hemispheric mixing of air. The simulated $\delta(\text{APO})$ underestimated the observed interannual variation in $\delta(\text{APO})$ significantly, probably due to the
20 interannual variation in the annual mean air-sea O_2 flux. Interannual variation in $\delta(\text{APO})$ driven by the net marine biological activities, obtained by subtracting the assumed solubility-driven component of $\delta(\text{APO})$ from the total variation, indicated a clear evidence of influence on annual sea-to-air (air-to-sea) marine biological O_2 flux during El Niño (La Niña). By analyzing the observed secular trends of $\delta(\text{O}_2/\text{N}_2)$ and CO_2 amount fraction, global average terrestrial biospheric and oceanic CO_2 uptakes for the period 2012–2019 were estimated to be (1.8 ± 0.9) and (2.8 ± 0.6) Pg a^{-1} (C equivalents), respectively.

25

1 Introduction

Atmospheric O_2/N_2 ratio has been observed since the early 1990s, not only for separating out terrestrial biospheric and oceanic CO_2 uptakes, but also for evaluating marine biospheric activities (Keeling and Shertz, 1992). For this purpose, observations of the O_2/N_2 ratio have been carried out at many surface stations and on commercial cargo ships (e.g., Bender et al., 2005; Manning and Keeling, 2006; Tohjima et al., 2008, 2019; Goto et al., 2017). The O_2/N_2 ratio varies in opposite phase
30



with CO₂ amount fraction due to the terrestrial biospheric activities and fossil fuel combustion, of which respective O₂:CO₂ exchange ratios (oxidative ratio (OR) = $-\Delta y(\text{O}_2)\Delta y(\text{CO}_2)^{-1}$ mol mol⁻¹) are about 1.1 and 1.4, respectively (Keeling, 1988; Severinghaus, 1995), where y stands for the dry amount fraction of gas, as recommended by the IUPAC Green Book (2007). By using the OR value of 1.1 for terrestrial biospheric activities, Atmospheric Potential Oxygen (APO) is defined by $y(\text{APO}) = y(\text{O}_2) + 1.1y(\text{CO}_2)$ (Stephens et al., 1998). While APO is conserved for terrestrial biospheric activities, the air-sea exchange of O₂ is much faster than that of CO₂ since the air-sea CO₂ exchange is highly suppressed by a carbon dissociation effect in seawater (e.g. Keeling et al., 1993). Therefore, APO can be used to evaluate air-sea O₂ fluxes associated with marine biological and physical processes (e.g. Nevison et al., 2012). From this point of view, aircraft observation serves as a useful platform for measuring altitude-dependent APO driven by spatially-integrated air-sea O₂ fluxes at the surface.

Aircraft observations of the O₂/N₂ ratio have been conducted in the past (e.g. Sturm et al., 2005; Ishidoya et al., 2008a, 2012, 2014; van der Laan et al., 2014; Morgan et al., 2019; Birner et al., 2020; Stephens et al., 2018, 2021). Sturm et al. (2005) observed a vertical gradient and seasonal cycle in the O₂/N₂ ratio in the height range of 0.8-3.1 km over Perthshire, United Kingdom, for the period 2003-2004. Longer term observations of the tropospheric O₂/N₂ ratio have also been carried out by Ishidoya et al. (2012) and van der Laan et al. (2014). They conducted aircraft observations at heights of 2, 4 and above 8 km over Japan during 1999-2010 and at heights of 0.1 and 3 km over western Russia during 1998-2008, respectively, and provided additional evidence of seasonal cycles and secular changes in the tropospheric O₂/N₂ ratio. However, there were uncertainties associated with artificial fractionations of O₂ and N₂ in Ishidoya et al. (2012) and van der Laan et al. (2014). Ar/N₂ ratio and/or stable isotopic ratios can be used to evaluate natural and artificial molecular-diffusive fractionations of O₂ and N₂ (e.g. Kawamura et al., 2006; Ishidoya et al., 2013), however Ishidoya et al. (2012) and van der Laan et al. (2014) did not observe them.

Ishidoya et al. (2014) and Stephens et al. (2021) observed O₂/N₂ and Ar/N₂ simultaneously, and were able to correct for thermally-diffusive artificial fractionation on O₂/N₂, by using coefficients of 3.54 and 3.77 of Ar/O₂, respectively. By using the corrected O₂/N₂ ratio, Ishidoya et al. (2014) were able to observe spatiotemporal variations in the O₂/N₂ ratio from the surface to the middle troposphere over the Western North Pacific around Japan, on monthly scheduled flights, for the period May 2012 to April 2013. Similarly, Stephens et al. (2021) were able to provide a better picture of much wider-area distributions of O₂/N₂ ratio, from 0–14 km and 87° N to 85° S, using measurements from a series of aircraft campaigns such as five HIAPER Pole-to-Pole Observations campaigns (HIPPO) in 2009-2011 (Wofsy et al., 2011), and the O₂/N₂ Ratio and CO₂ Airborne Southern Ocean (ORCAS) study in 2016 (Stephens et al., 2018).

Stephens et al. (2021) also conducted continuous observations of O₂ mole fraction using a vacuum ultraviolet (VUV) absorption detector (Stephens et al., 2003). They adjusted the continuous O₂ data to the simultaneously observed flask-based O₂/N₂ ratio corrected for the artificial fractionation using Ar/N₂ ratio, since the artificial fractionations for the continuous observations were more significant than that for the flask sampling due to the lower flow rate. Based on the continuous O₂ data, Morgan et al. (2019) reported summertime vertical gradients of the atmospheric O₂/N₂ ratio and CO₂ amount fraction through the atmospheric boundary layer over the Drake Passage region of the Southern Ocean, to evaluate the air-sea O₂/CO₂



65 flux ratios in the region. Aircraft observations of Ar/N₂ are also used to evaluate gravitational separation of the atmospheric components, which is an indicator of the Brewer-Dobson circulation (e.g. Ishidoya et al., 2013), in the lowermost stratosphere under the condition that the artificial fractionation is reduced sufficiently (Ishidoya et al., 2008; Birner et al., 2020).

In this study, as an update to Ishidoya et al. (2014), we present 9-year-long O₂/N₂ ratio variations observed in the troposphere over the Western North Pacific. Measurements were carried out on monthly scheduled cargo aircraft flights with a fixed flight route, and the thermally-diffusive artificial fractionations on O₂/N₂ ratio were corrected by using simultaneously-measured Ar/N₂ ratio. Using these corrected values, we made precise evaluation of the high-latitude distributions of seasonal cycle, vertical profile and year-to-year variation along the flight route. We mainly focus our discussions on the variations in the tropospheric APO and CO₂ amount fraction with the aid of a 3-D atmospheric chemistry-transport model. We also estimate average terrestrial biospheric and oceanic CO₂ uptakes for the period 2012–2019, by using long-term trends of O₂/N₂ ratio and CO₂ amount fraction.

2 Method

The cargo aircraft C-130 flies once per month from Atsugi Base (35.45° N, 139.45° E), Kanagawa, Japan, to Minamitorishima (MNM; 24.28° N, 153.98° E), a small coral island, Japan. The flight altitude is about 6 km, and 24 air samples were pressurized into 1.7 L silica-coated Titanium flasks to an absolute pressure of 0.4 MPa during the flight. A set of 17–20 samples were collected during the level flight while others were collected during the descent portion at MNM. Details of the air sampling method has been described elsewhere (Tsuboi et al., 2013; Niwa et al., 2014). The flask air samples were brought back to the Japan Meteorological Agency (JMA) and analyzed for CO₂, CH₄, CO and N₂O amount fractions. The CO₂ amount fraction was measured using a non-dispersive infrared analyzer (Licor, LI-7000) with a precision of better than ±0.07 ppm (Tsuboi et al., 2013). The dataset is posted on the WMO's World Data Centre for Greenhouse Gases (WMO/WGCGG, <http://ds.data.jma.go.jp/gmd/wdcgg/wdcgg.html>). After the JMA analyses, the flasks were sent to the National Institute of Advanced Industrial Science and Technology (AIST) to measure O₂/N₂ and Ar/N₂ ratios, as well as the stable isotopic ratios of N₂, O₂ and Ar (Ishidoya et al., 2014). In this study, we present the measured data obtained from the air samples collected for the period May 2012 – March 2020. In Fig. 1, we show all the locations where the air samples were collected onboard C-130 aircrafts during the observation period, and the locations of MNM, Atsugi Base and Ioto Island (24.76° N, 141.29° E), Japan.

The values of $\delta(\text{O}_2/\text{N}_2)$, $\delta(\text{Ar}/\text{N}_2)$, stable isotopic ratios of N₂, O₂ and Ar ($\delta(^{15}\text{N})$, $\delta(^{18}\text{O})$ and $\delta(^{40}\text{Ar})$) are reported in per meg (one per meg is equal to 1×10^{-6}):

$$\delta(\text{O}_2/\text{N}_2) = \frac{R_{\text{sample}}(^{16}\text{O}^{16}\text{O}/^{14}\text{N}^{14}\text{N})}{R_{\text{standard}}(^{16}\text{O}^{16}\text{O}/^{14}\text{N}^{14}\text{N})} - 1, \quad (1)$$

$$\delta(\text{Ar}/\text{N}_2) = \frac{R_{\text{sample}}(^{40}\text{Ar}/^{14}\text{N}^{14}\text{N})}{R_{\text{standard}}(^{40}\text{Ar}/^{14}\text{N}^{14}\text{N})} - 1, \quad (2)$$



$$95 \quad \delta(^{15}\text{N}) = \frac{R_{\text{sample}}(^{15}\text{N}^{14}\text{N}/^{14}\text{N}^{14}\text{N})}{R_{\text{standard}}(^{15}\text{N}^{14}\text{N}/^{14}\text{N}^{14}\text{N})} - 1, \quad (3)$$

$$\delta(^{18}\text{O}) = \frac{R_{\text{sample}}(^{18}\text{O}^{16}\text{O}/^{16}\text{O}^{16}\text{O})}{R_{\text{standard}}(^{18}\text{O}^{16}\text{O}/^{16}\text{O}^{16}\text{O})} - 1, \quad (4)$$

$$\delta(^{40}\text{Ar}) = \frac{R_{\text{sample}}(^{40}\text{Ar}/^{36}\text{Ar})}{R_{\text{standard}}(^{40}\text{Ar}/^{36}\text{Ar})} - 1, \quad (5)$$

where the subscripts ‘sample’ and ‘standard’ refer to the values of the sample and standard air, respectively. The values of $\delta(\text{O}_2/\text{N}_2)$, $\delta(\text{Ar}/\text{N}_2)$, $\delta(^{15}\text{N})$, $\delta(^{18}\text{O})$ and $\delta(^{40}\text{Ar})$ of the air samples were determined against our primary standard air (cylinder
100 No. CRC00045) by using a mass spectrometer (Thermo Scientific Delta-V) (Ishidoya and Murayama, 2014) with a respective reproducibility of about 5, 8, 1, 3 and 13 per meg (1σ).

As already discussed in Ishidoya et al. (2014), the measured values of $\delta(\text{O}_2/\text{N}_2)$ are contaminated by significant artificial thermally-diffusive fractionation of O_2 and N_2 during the air sample collection process onboard the aircraft. Figure 2 shows the relationships between $\delta(\text{Ar}/\text{N}_2)$, $\delta(^{18}\text{O})$ and $\delta(^{40}\text{Ar})$ with $\delta(^{15}\text{N})$ for all the air samples analyzed in this study. It was
105 found that $\delta(\text{Ar}/\text{N}_2)$, $\delta(^{18}\text{O})$ and $\delta(^{40}\text{Ar})$ change linearly in proportion to $\delta(^{15}\text{N})$, and the linear regression analyses gave respective slopes of (16.3 ± 0.1) , (1.58 ± 0.01) and (2.69 ± 0.05) per meg per meg⁻¹ for the $\delta(\text{Ar}/\text{N}_2)/\delta(^{15}\text{N})$, $\delta(^{18}\text{O})/\delta(^{15}\text{N})$ and $\delta(^{40}\text{Ar})/\delta(^{15}\text{N})$ ratios. These ratios agree well with the ratios of (16.2 ± 0.1) , (1.55 ± 0.02) and (2.75 ± 0.05) for $\delta(\text{Ar}/\text{N}_2)/\delta(^{15}\text{N})$, $\delta(^{18}\text{O})/\delta(^{15}\text{N})$ and $\delta(^{40}\text{Ar})/\delta(^{15}\text{N})$, respectively, determined from the laboratory experiments on the effect of thermally-diffusive
110 diffusive fractionation of O_2 and N_2 on the observed $\delta(\text{O}_2/\text{N}_2)$ by using the following equation (Ishidoya et al., 2014):

$$\delta_{\text{cor.}}(\text{O}_2/\text{N}_2) = \delta_{\text{meas.}}(\text{O}_2/\text{N}_2) - \alpha_{\text{O}_2} \cdot \alpha_{\text{Ar}}^{-1} \cdot \Delta\delta_{\text{meas.}}(\text{Ar}/\text{N}_2), \quad (6)$$

Here, $\delta_{\text{cor.}}(\text{O}_2/\text{N}_2)$ and $\delta_{\text{meas.}}(\text{O}_2/\text{N}_2)$ denote the corrected and measured $\delta(\text{O}_2/\text{N}_2)$, respectively. The coefficients $\alpha_{\text{O}_2} = (4.57 \pm 0.02)$ and $\alpha_{\text{Ar}} = (16.2 \pm 0.1)$ are the $\delta(\text{O}_2/\text{N}_2)/\delta(^{15}\text{N})$ and $\delta(\text{Ar}/\text{N}_2)/\delta(^{15}\text{N})$ ratios respectively, determined from the laboratory experiments as described by Ishidoya et al. (2013). $\Delta\delta_{\text{meas.}}(\text{Ar}/\text{N}_2)$ is the deviation of the measured $\delta(\text{Ar}/\text{N}_2)$ from
115 its reference point that is determined by using the annual mean value of $\delta(\text{Ar}/\text{N}_2)$ in 2013 observed at the surface in Tsukuba (36°N , 140°E), Japan (Ishidoya and Murayama, 2014). The overall uncertainty of $\delta_{\text{cor.}}(\text{O}_2/\text{N}_2)$ was evaluated to be less than 6 per meg, and the effect of the seasonal $\delta(\text{Ar}/\text{N}_2)$ cycle on $\delta_{\text{cor.}}(\text{O}_2/\text{N}_2)$ was not therefore excluded in this study; this could lead to an over (under)-correction of the surface $\delta_{\text{cor.}}(\text{O}_2/\text{N}_2)$ by about 2 per meg in the summertime (wintertime). The details of the correction of artificial fractionations of O_2 and N_2 is given in Ishidoya et al. (2014). Figure 3(a) shows the measured
120 $\delta(\text{O}_2/\text{N}_2)$ and $\delta(\text{Ar}/\text{N}_2)$ for all the air samples observed in this study, and Fig. 3(b) shows the $\delta_{\text{cor.}}(\text{O}_2/\text{N}_2)$ corrected values by applying eq. (6) to the measured values. As seen from the figures, significant artificial fractionations found in the measured $\delta(\text{O}_2/\text{N}_2)$ are reduced dramatically by the correction. It can also be seen from Fig. 3(a) that the fractionations have become smaller since 2018, but were larger at the higher altitude before 2018. It should be noted that these noted changes across 2018



could be at least partly related to changes in the aircraft type from C-130H to C-130R used for flask sampling. However, no
125 systematic data gaps were found in the $\delta_{\text{cor.}}(\text{O}_2/\text{N}_2)$ time series across 2018.

We used $\delta(\text{APO})$ for the detail analyses of the air-sea exchange of O_2 . $\delta(\text{APO})$ was calculated from the observed
 $\delta_{\text{cor.}}(\text{O}_2/\text{N}_2)$ and CO_2 amount fraction in per meg;

$$\delta(\text{APO}) = \delta_{\text{cor.}}(\text{O}_2/\text{N}_2) + \frac{\alpha_{\text{B}}}{X_{\text{O}_2}} y(\text{CO}_2) \times 10^6 - 2000, \quad (7)$$

where $y(\text{CO}_2)$ is the dry amount fraction of CO_2 , α_{B} is the OR of 1.1 for terrestrial biospheric activities, X_{O_2} of 0.2093 is the
130 amount fraction of atmospheric O_2 (Aoki et al., 2019), and 2000 is an arbitrary reference. From the definition, $\delta(\text{APO})$ is
conserved for terrestrial biospheric activities, but not so for air-sea exchange of O_2 , N_2 and CO_2 , and fossil fuel consumption
and have an average OR value that is larger than 1.1 (Keeling, 1988). In order to investigate the observed $\delta_{\text{cor.}}(\text{O}_2/\text{N}_2)$ variations,
we used a three-dimensional atmospheric transport model NICAM-TM (Niwa et al., 2011) to simulate CO_2 amount fraction
and $\delta(\text{APO})$ using surface O_2 , N_2 and CO_2 fluxes. NICAM-TM is based on the Nonhydrostatic ICosahedral Atmospheric
135 Model (NICAM: Satoh et al., 2008, 2014) and its tracer transport version has been used for atmospheric transport and flux
inversion studies of greenhouse gases (e.g. Niwa et al. 2012). The horizontal model resolution used in this study had a mean
grid interval of about 112 km. The model was driven by nudging the horizontal winds towards the Japanese 55-year Reanalysis
data (JRA-55: Kobayashi et al., 2015).

The surface fluxes incorporated into NICAM-TM were the air-sea fluxes of O_2 , N_2 and CO_2 , and also CO_2 and O_2 fluxes
140 from fossil fuel combustion. The air-sea O_2 and N_2 fluxes were the climatological monthly anomalies taken from the TransCom
experimental protocol (Blain, 2005; Garcia and Keeling 2001). The fluxes were computed to give the seasonal component and
the annual mean values at every grid point to be zero. The air-sea CO_2 flux was obtained from the monthly sea surface CO_2
flux climatology of Takahashi et al. (2009). The CDIAC fossil fuel database was used for the fossil fuel CO_2 flux (Andres et
al., 2016; Gilfillan et al., 2019). Model-based $\delta(\text{APO})$, CO_2 amount fraction and $\delta(\text{O}_2/\text{N}_2)$ were calculated using the following
145 equations (e.g. Tohjima et al., 2012) in per meg, ppm and per meg, respectively:

$$\delta(\text{APO}) = \left(\frac{y^{\text{SA}}(\text{O}_2)}{X_{\text{O}_2}} - \frac{y^{\text{SA}}(\text{N}_2)}{X_{\text{N}_2}} \right) + \left(\frac{-\alpha_{\text{F}} y^{\text{FF}}(\text{CO}_2) + \alpha_{\text{B}} y^{\text{FF}}(\text{CO}_2)}{X_{\text{O}_2}} \right) + \frac{\alpha_{\text{B}} y^{\text{OC}}(\text{CO}_2)}{X_{\text{O}_2}}, \quad (8)$$

$$y(\text{CO}_2) = y^{\text{FF}}(\text{CO}_2) + y^{\text{OC}}(\text{CO}_2) + y^{\text{TB}}(\text{CO}_2), \quad (9)$$

$$\delta(\text{O}_2/\text{N}_2) = \left(\frac{y^{\text{SA}}(\text{O}_2)}{X_{\text{O}_2}} - \frac{y^{\text{SA}}(\text{N}_2)}{X_{\text{N}_2}} \right) + \frac{-\alpha_{\text{F}} y^{\text{FF}}(\text{CO}_2)}{X_{\text{O}_2}} + \frac{-\alpha_{\text{F}} y^{\text{TB}}(\text{CO}_2)}{X_{\text{O}_2}}, \quad (10)$$

where $y(\text{O}_2)$, $y(\text{N}_2)$ and $y(\text{CO}_2)$ are dry amount fractions of the respective gases calculated using NICAM-TM. The superscripts
150 “SA”, “FF”, “OC” and “TB” denote the seasonal anomaly, CO_2 flux from fossil fuel combustion, ocean and terrestrial
biosphere, respectively. X_{O_2} and α_{B} have the same meaning as in Equation (7), while X_{N_2} is the dry amount fraction of N_2
in the atmosphere and α_{F} is the global average OR for fossil fuel combustion. In this study, we adopted $X_{\text{N}_2} = 0.7808$ and $\alpha_{\text{F}} =$
1.35 (e.g. Keeling and Manning, 2014). We can rewrite equation (8) as:

$$\delta(\text{APO}) = \delta^{\text{SA}}(\text{APO}) + \delta^{\text{FF}}(\text{APO}) + \delta^{\text{OC}}(\text{APO}). \quad (11)$$



155 The $\delta(\text{APO})$ simulation run incorporating the above-mentioned surface fluxes is referred to as the “control run”. In this calculation, $\delta(\text{APO})$ driven by an annual mean air-sea O_2 and N_2 fluxes (hereafter referred to as the “ $\delta^{\text{AM}}(\text{APO})$ ”) that was considered by Tohjima et al. (2012) was ignored. However, the contribution of $\delta^{\text{AM}}(\text{APO})$ was evaluated by subtracting the simulated $\delta(\text{APO})$ from the observed $\delta(\text{APO})$, for interannual variation in Sections 3-2.

3 Results and discussion

160 3.1 Latitudinal and vertical distributions of $\delta_{\text{cor.}}(\text{O}_2/\text{N}_2)$, CO_2 amount fraction and $\delta(\text{APO})$

Figure 4(a) shows variations in the $\delta_{\text{cor.}}(\text{O}_2/\text{N}_2)$, CO_2 amount fraction and $\delta(\text{APO})$ observed in the layer (6.1 ± 0.5) km ($\pm 1\sigma$) (hereafter referred to as “middle troposphere”) at five latitudes over the western North Pacific. Best-fitted curves to the data and secular trends obtained using a digital filtering technique (Nakazawa et al., 1997a) are also shown. In the filtering technique, the average seasonal cycles were approximated by fundamental and its first harmonics, and signals with periods longer than 36 months were regarded as contributing to a secular trend. As can be seen in Fig. 4(a), secular decreases in $\delta_{\text{cor.}}(\text{O}_2/\text{N}_2)$ and $\delta(\text{APO})$ and increases in CO_2 amount fraction, accompanied by prominent seasonal cycles, were observed at each latitude. The secular changes in $\delta_{\text{cor.}}(\text{O}_2/\text{N}_2)$ and CO_2 amount fraction can be attributed mainly to O_2 consumption and CO_2 emission resulting from fossil fuel combustion. The seasonally dependent air-sea O_2 flux and the terrestrial biospheric activity contribute towards the observed seasonal $\delta(\text{O}_2/\text{N}_2)$ cycle, while the terrestrial biospheric activity is the main contributor to the seasonal CO_2 amount fraction cycle (e.g. Keeling et al., 1993; Keeling and Manning, 2014). The average rates of change in the observed $\delta_{\text{cor.}}(\text{O}_2/\text{N}_2)$, CO_2 amount fraction and $\delta(\text{APO})$ at the four latitudes shown in Fig. 4(a) were (-24.2 ± 0.4) per meg a^{-1} , (2.43 ± 0.05) ppm a^{-1} and (-11.3 ± 0.4) per meg a^{-1} , respectively, for the observational period. General features of the observed variations in $\delta(\text{O}_2/\text{N}_2)$, CO_2 amount fraction and $\delta(\text{APO})$ are well reproduced by the control run of NICAM-TM, as shown in Fig. 4(b). Figure 5(a) shows variations in $\delta_{\text{cor.}}(\text{O}_2/\text{N}_2)$, CO_2 amount fraction and $\delta(\text{APO})$ observed over MNM. Clear secular trends and prominent seasonal cycles of $\delta_{\text{cor.}}(\text{O}_2/\text{N}_2)$, CO_2 amount fraction and $\delta(\text{APO})$ are distinguishable, similar to those in Fig. 4(a). We also note in the figure that the seasonal amplitudes of $\delta_{\text{cor.}}(\text{O}_2/\text{N}_2)$, CO_2 amount fraction and $\delta(\text{APO})$ decrease with increasing altitudes. These features are also reproduced by the control run of NICAM-TM (Fig. 5(b)).

Figure 6(a) shows average seasonal cycles of $\delta(\text{APO})$ and CO_2 amount fraction observed at five latitudes over the western North Pacific. They show clear seasonal cycles with summertime maxima in $\delta(\text{APO})$ and minima in CO_2 . However, the amplitude of seasonal $\delta(\text{APO})$ cycle decreases significantly toward the lower latitudes, with seasonal maxima and minima clearly occurring earlier than those of the CO_2 cycle. Figure 6(b) shows the corresponding average seasonal cycles of $\delta(\text{APO})$ and CO_2 amount fraction obtained from the control run of NICAM-TM. Earlier appearances of the seasonal maxima and minima in $\delta(\text{APO})$ than those in CO_2 amount fraction are reproduced by NICAM-TM. The seasonal amplitude of the simulated



$\delta(\text{APO})$ also decreases toward the lower latitudes, in agreement with the observation, but is underestimated. As for the CO_2 amount fraction, the simulated seasonal cycles agree well with the observations.

Figure 7(a) shows average seasonal cycles of $\delta(\text{APO})$ and CO_2 amount fraction observed over MNM. The $\delta(\text{APO})$ seasonal cycle varies in opposite phase from the CO_2 amount fraction. However, amplitudes of the seasonal $\delta(\text{APO})$ cycle decrease significantly with the higher altitude, with seasonal minima clearly occurring earlier than those of the CO_2 cycle. These salient characteristics are reproduced generally by the NICAM-TM control run (Fig. 7(b)).

In order to identify and explore some of the cause(s) that gave rise to the observed differences in the latitudinal/altitudinal changes in the seasonal cycles between $\delta(\text{APO})$ and CO_2 amount fraction shown in Fig. 6(a) and 7(a), we carried out additional NICAM-TM simulations. In the calculation, we used the same fluxes that were used in the control run but for the northern hemispheric flux only for the TransCom seasonal climatology (hereafter referred to as “w/o SH flux run”). It is well known that the anti-phase nature of the seasonal $\delta(\text{APO})$ cycles between the northern and southern hemispheres is due to seasonal changes in the air-sea O_2 (N_2) flux with summertime maxima (e.g. Keeling et al., 1998; Tohjima et al., 2012). Therefore, in comparing the control run with the w/o SH flux run, we decided to evaluate changes in the seasonal $\delta(\text{APO})$ cycle by superimposing the anti-phase seasonal cycles through the inter-hemispheric mixing of air. On the other hand, seasonal CO_2 amount fraction cycle is much smaller in the southern hemisphere than that in the northern hemisphere (e.g. Nakazawa et al., 1997b). Therefore, it is expected that the seasonal CO_2 amount fraction cycle in the northern hemisphere does not change significantly by the inter-hemispheric atmospheric mixing.

The seasonal $\delta(\text{APO})$ cycles obtained from the w/o SH flux run are also shown in Figs. 6(b) and 7(b). As seen from Fig. 6(b), latitudinal differences in the seasonal $\delta(\text{APO})$ amplitudes from the w/o SH flux run are clearly smaller than those from the control run. In addition, appearances of the maxima and minima of the seasonal $\delta(\text{APO})$ cycle from the w/o SH flux run are later than those from the control run, pushing the timing closer to those of seasonal CO_2 amount fraction cycles. The seasonal $\delta(\text{APO})$ cycles from the w/o SH flux run in Fig. 7(b) also show similar features. These results suggest that the inter-hemispheric mixing of air modifies the seasonal $\delta(\text{APO})$ cycles significantly, especially in the higher altitude in the lower latitude region. To compare, in more detail, the observed latitudinal/altitudinal variation in the seasonal $\delta(\text{APO})$ cycle amplitude with those calculated by NICAM-TM, Fig. 8(a) shows a latitudinal distribution of average fractions of the observed seasonal $\delta(\text{APO})$ and CO_2 amount fraction amplitudes relative to the 33.5° N values. The decrease in the seasonal amplitude of $\delta(\text{APO})$ toward the lower latitude is about 50%, while that of CO_2 amount fraction is less than 10%; these are well reproduced by the control run of NICAM-TM. On the other hand, the w/o SH flux run yields a decrease in the $\delta(\text{APO})$ amplitude by 20% toward the lower latitude, which is significantly smaller than that from the $\delta(\text{APO})$ from control run, but slightly larger than that of CO_2 amount fraction. Therefore, these results support the idea that the observed latitudinal changes in the seasonal amplitude of the middle tropospheric $\delta(\text{APO})$, from the mid-latitude to the subtropical region, are caused mainly by a superposition of the northern and southern hemispheric seasonal cycles through the inter-hemispheric mixing of air.



Figure 8(b) shows average fractions of the seasonal amplitudes of $\delta(\text{APO})$ and CO_2 amount fraction with height, relative to surface values. The surface seasonal cycles are obtained from continuous observations of $\delta(\text{O}_2/\text{N}_2)$ and CO_2 amount fraction at MNM since December 2015 (updated from Ishidoya et al., 2017). The seasonal amplitude of APO decreases rapidly with height by about 70%, while that of CO_2 amount fraction decreases by less than 20%. These features are well reproduced by the control run of NICAM-TM. The altitudinal decrease in the seasonal $\delta(\text{APO})$ amplitude is also reproduced by the w/o SH flux run, although a slight underestimation is found above 5 km. Therefore, the altitudinal decrease in the seasonal $\delta(\text{APO})$ amplitude over MNM is mainly due to an attenuation of the seasonal air-sea O_2 and N_2 fluxes around MNM with height, with some influence from the inter-hemispheric atmospheric mixing. Consequently, over the western North Pacific region, the height-latitude distribution of seasonal $\delta(\text{APO})$ cycles is highly sensitive to the atmospheric transport processes associated with inter-hemispheric air mixing and vertical attenuation of surface signal, compared with those of seasonal CO_2 amount fraction cycles.

We also compared the observed and simulated annual mean values of $\delta(\text{APO})$ and CO_2 amount fraction. Figure 9(a) shows average deviations of the middle tropospheric annual mean values of $\delta(\text{APO})$ and CO_2 amount fraction at each latitude, relative to the 25.5°N values. The deviation values of $\delta(\text{APO})$ and CO_2 amount fraction are well reproduced by the control and w/o SH flux runs. Therefore, the surface fluxes of O_2 , N_2 and CO_2 in the northern hemisphere are the main contributors to the observed latitudinal variations in Fig. 9(a). As discussed in connection with eq. (11), we ignored $\delta^{\text{AM}}(\text{APO})$ in our $\delta(\text{APO})$ simulation using NICAM-TM, which is a component of $\delta(\text{APO})$ driven by annual mean air-sea O_2 and N_2 fluxes. Therefore, the results of our simulation suggest that $\delta^{\text{AM}}(\text{APO})$ does not affect significantly the latitudinal variations in the annual mean values of the middle tropospheric $\delta(\text{APO})$ at $25\text{--}34^\circ \text{N}$. Figure 9(b) shows the height deviations of the annual mean values of $\delta(\text{APO})$ and CO_2 amount fraction, relative to their corresponding values at 6 km over MNM. The observed profile of CO_2 amount fraction is well reproduced by NICAM-TM. On the other hand, the average vertical gradient of $\delta(\text{APO})$ profiles, obtained from the control and w/o SH flux runs of NICAM-TM, seems to be slightly larger than the observation. This may be due to the ignored contribution of $\delta^{\text{AM}}(\text{APO})$; in that case, it may be that the sea area around MNM emits O_2 to the atmosphere throughout the observation period. Moreover, it is clearly seen from the figure that the interannual variation in the observed $\delta(\text{APO})$ profiles is much larger than that in the NICAM-TM simulations. This may also be due to the ignored contribution of $\delta^{\text{AM}}(\text{APO})$, and we discuss interannual variations in the observed and simulated $\delta(\text{APO})$ in the section below.

3.2 Interannual variations in $\delta(\text{APO})$ and its implication to global air-sea O_2 flux and CO_2 budget

In this section, we discuss causes of the interannual variations found in the middle tropospheric $\delta(\text{APO})$ observed over the western North Pacific. Figure 10 shows annual change rates of the middle tropospheric $\delta(\text{APO})$ at each latitude. The change rates observed at $29\text{--}34^\circ \text{N}$ show interannual variation with maxima around the early 2015 and mid 2019, with a minimum at



all latitudes in the early 2017. The corresponding change rates obtained from the control run of NICAM-TM are also shown in Fig. 10. The change rates obtained from NICAM-TM at 29–34° N show interannual variations in phase with the observed rates, although the amplitudes are smaller by about 80%. The interannual variations observed at 24–28° N are also larger than the simulated values. Therefore, it is likely that interannual variation in the $\delta^{\text{AM}}(\text{APO})$, which was not incorporated into
250 NICAM-TM, is a main contributor to the observed interannual variations at various latitudes. In this connection, it is possible that the interannual variation in the global air-sea CO₂ flux could also contribute to the larger interannual variation in the observed $\delta(\text{APO})$ since the NICAM-TM model incorporated only the monthly sea surface CO₂ flux climatology to calculate $\delta^{\text{C}}(\text{APO})$. However, the global air-sea CO₂ flux reported by the Global Carbon Project (GCP) (Friedlingstein et al., 2020)
255 showed an interannual variation of 0.07 Pg a⁻¹ during 2012–2019, corresponding to 0.2 per meg a⁻¹ of $\delta^{\text{C}}(\text{APO})$, which is much smaller than the interannual variation in the observed $\delta(\text{APO})$ shown in Fig. 10.

By assuming that all other components besides $\delta^{\text{AM}}(\text{APO})$ are well represented in the NICAM-TM control run, we subtracted the change rates simulated by NICAM-TM from the observed rates, to extract the interannual variations due only to the $\delta^{\text{AM}}(\text{APO})$. The calculated change rates of $\delta^{\text{AM}}(\text{APO})$ are shown at the bottom of Fig. 10. The change rates show similar
260 interannual variations to the observed rates, but the latitudinal differences are smaller. This suggests that the interannual variations driven by $\delta^{\text{AM}}(\text{APO})$ do not differ significantly as a function of latitude. In the following discussion, we make a bold assumption that an average of the change rates of $\delta^{\text{AM}}(\text{APO})$ shown in Fig. 10 as a global average.

An anomaly of the average interannual variation of $\delta^{\text{AM}}(\text{APO})$ change rate is shown in Fig. 11 (black line). In this figure, we also plotted a similar anomaly of interannual variation of the $\delta(\text{APO})$ change rate due to solubility change (red line, hereafter referred to as “ $\delta_{\text{herm}}(\text{APO})$ ”). The $\delta_{\text{herm}}(\text{APO})$ was calculated from the $\delta(\text{Ar}/\text{N}_2)$ measurements observed at Tsukuba (36° N,
265 140° E), Japan (Ishidoya et al., 2021), by multiplying a coefficient of 0.84 derived from differences in the solubility in O₂ and Ar (Weiss 1970; Blaine, 2005). As discussed in Ishidoya et al. (2021), the interannual variation in the $\delta(\text{Ar}/\text{N}_2)$ change rate is in phase with the global ocean heat content reported by ocean temperature measurements (e.g. Levitus et al., 2012). This suggests that $\delta_{\text{herm}}(\text{APO})$ is also driven by changes in the solubility of the global seawater. By subtracting $\delta_{\text{herm}}(\text{APO})$ from
270 $\delta^{\text{AM}}(\text{APO})$, we estimated interannual variation of the $\delta(\text{APO})$ change rate due to marine biological activities (green line, hereafter referred to as “ $\delta_{\text{netbio}}(\text{APO})$ ”). It is expected that $\delta_{\text{netbio}}(\text{APO})$ is driven by marine biological activities, not only in the surface mixed layer but also through a ventilation of subsurface low-O₂ waters.

Both the $\delta_{\text{herm}}(\text{APO})$ and $\delta_{\text{netbio}}(\text{APO})$ show significant interannual variations, roughly in opposite phase with each other. Moreover, the change rate of $\delta_{\text{netbio}}(\text{APO})$ varies in opposite phase with the NINO.WEST (Japan Meteorological Agency,
275 https://www.data.jma.go.jp/gmd/cpd/db/el_nino/index/ninowidx.html), which is an index of El Niño–Southern Oscillation (ENSO). The ENSO is in the El Niño and La Niña phase, respectively, during the period with the negative and positive NINO.WEST index. Therefore, the $\delta_{\text{netbio}}(\text{APO})$ tends to increase and decrease during El Niño and La Niña, respectively. This is consistent with Eddebber et al. (2017) who examined global and tropical air-sea O₂ flux responses to ENSO, based on the Community Earth System Model (CESM). They reported that the upper ocean loses O₂ to the atmosphere during El Niño and



280 gains O₂ during La Niña mainly due to changes in ventilation of low-O₂ waters in the tropical Pacific, the region that has a dominant influence over the interannual variation in global air-sea O₂ flux (McKinley et al., 2003). By assuming the interannual variation in the $\delta_{\text{netbio}}(\text{APO})$ represents a global average, and assuming a 1-box atmosphere with 5.124×10^{21} g for the total mass of dry air (Trenberth, 1981), 28.97 g mol^{-1} for the mean molecular weight of dry air, and respective fractions of 0.2093 and 0.7808 for O₂ and N₂ in the atmosphere, we estimated an interannual variation in the global air-sea O₂ flux due to marine
285 biological activities (right axis of the green line in Fig. 12). The peak-to-peak amplitude of the O₂ flux is found to be about 300 Tmol yr⁻¹, which is almost consistent with that of global APO flux estimated using the $\delta(\text{APO})$ data from Scripps stations (Keeling and Manning, 2014) and a global atmospheric transport inversion (Rödenbeck et al., 2008; Eddebber et al., 2017).

By assuming the average secular trends of the middle tropospheric $\delta_{\text{cor}}(\text{O}_2/\text{N}_2)$ and CO₂ amount fraction observed in this study to be global average values, we were able to estimate the global CO₂ budget. The equations for separating out the
290 global net terrestrial biospheric and oceanic CO₂ uptake are given by Keeling and Shretz (1992) firstly as;

$$B = \frac{\alpha_F}{\alpha_B} F + \frac{1}{0.471} \frac{X_{\text{O}_2}}{\alpha_B} \frac{d\delta(\text{O}_2/\text{N}_2)}{dt} - \frac{Z_{\text{eff}}}{\alpha_B}, \quad (12)$$

and

$$O = -\frac{1}{0.471} \frac{d}{dt} \left(y(\text{CO}_2) + \frac{X_{\text{O}_2}}{\alpha_B} \delta(\text{O}_2/\text{N}_2) \right) + \frac{\alpha_B - \alpha_F}{\alpha_B} F + \frac{Z_{\text{eff}}}{\alpha_B}. \quad (13)$$

295 Here, B , F and O (in Pg yr⁻¹, C equivalents) are the global terrestrial biospheric CO₂ uptake, the anthropogenic CO₂ emitted from fossil fuel combustion and cement manufacturing, and the oceanic CO₂ exchange, respectively; $d\delta(\text{O}_2/\text{N}_2)dt^{-1}$ (per meg a⁻¹) and $dy(\text{CO}_2)dt^{-1}$ (ppm a⁻¹) are the observed change rates in atmospheric $\delta_{\text{cor}}(\text{O}_2/\text{N}_2)$ and CO₂ amount fraction, respectively; 0.471 converts CO₂ emissions of 1 Pg to ppm of atmospheric CO₂; X_{O_2} is the standard mole fraction of O₂ in air (0.2093), α_F and α_B are the OR for global average fossil fuel combustion and net terrestrial biospheric activities, respectively; and Z_{eff} (Pg
300 yr⁻¹) represents the net effect of oceanic O₂ outgassing on the oceanic and terrestrial biospheric CO₂ uptakes, which has been considered since Bender et al. (2005) and Manning and Keeling (2006). α_F was calculated to be 1.37 from the fossil fuel and cement production emissions by fuel type for the period 2012-2019, reported by GCP (Friedlingstein et al., 2020), and the oxidative ratios for the different fuel type were taken from Keeling (1988).

Long-term change in Z_{eff} is caused mainly by stratification of the ocean and the decrease of O₂ solubility in seawater due
305 to a secular increase in the global ocean heat content (e.g., Bopp et al., 2002). However, as discussed above for Fig. 11, the ocean O₂ outgassing shows significant interannual variation, which makes it difficult to estimate year-to-year variations in the global CO₂ budget from eqs. (12) and (13). In this regard, Tohjima et al. (2019) estimated the terrestrial biospheric and the oceanic CO₂ uptakes using their $\delta(\text{O}_2/\text{N}_2)$ and CO₂ amount fraction data, by changing the time period to obtain average secular change rates. They reported that the CO₂ uptakes estimated by using the change rates averaged over a longer period greater
310 than 5 years were consistent with those reported by GCP (Le Quéré et al., 2018) within $\pm 0.5 \text{ Pg a}^{-1}$, while those estimated using annual change rates scattered significantly.



It seems that the averaging period needed to reduce the interannual variations in $\delta_{\text{therm}}(\text{APO})$ and $\delta_{\text{netbio}}(\text{APO})$ in Fig. 11, is about 4-5 years, similar to Tohjima et al. (2019). Therefore, we estimated average terrestrial biospheric and oceanic CO_2 uptake throughout the observation period (2012-2019; 8-year) to reduce the interannual variation in Z_{eff} sufficiently. By using the global ocean (0-2000 m) heat content data from the National Oceanographic Data Center (NOAA)/National Centers for Environmental Information (NCEI) (updated from Levitus et al. 2012, https://www.nodc.noaa.gov/OC5/3M_HEAT_CONTENT/) and the same ratio of air-sea O_2 (N_2) flux to air-sea heat flux used in Manning and Keeling (2006), we adopted $(0.6 \pm 0.6) \text{ Pg a}^{-1}$ for Z_{eff} for the period 2012-2019. We assumed 100% uncertainty for Z_{eff} following Manning and Keeling (2006). The value of F , $(9.7 \pm 0.5) \text{ Pg a}^{-1}$, was obtained from emissions from fossil fuel combustion and industrial processes by GCP (Friedlingstein et al., 2020). By using the average secular trends of $\delta_{\text{cor.}}(\text{O}_2/\text{N}_2)$ and CO_2 amount fraction for the observational period of the present study, the respective terrestrial biospheric and oceanic CO_2 uptakes were estimated to be (1.8 ± 0.9) and $(2.8 \pm 0.6) \text{ Pg a}^{-1}$ for the period 2012-2019. These values agree well with the corresponding CO_2 uptake of (1.8 ± 1.1) and $(2.6 \pm 0.5) \text{ Pg a}^{-1}$ reported by the GCP (Friedlingstein et al. 2020). It is noted that the terrestrial biospheric CO_2 uptake by GCP is calculated by subtracting the CO_2 emission due to land-use change $((1.6 \pm 0.7) \text{ Pg a}^{-1})$ from their estimated total land CO_2 uptake $((3.4 \pm 0.9) \text{ Pg a}^{-1})$.

4 Conclusions

Cargo aircraft C-130 flies once per month from Atsugi Base to MNM, and air samples have been collected during the level flight and during the descent portion at MNM. In this paper, we have presented the analytical results of the air samples for CO_2 amount fraction, $\delta(\text{O}_2/\text{N}_2)$, $\delta(\text{Ar}/\text{N}_2)$, $\delta(^{15}\text{N})$ of N_2 , $\delta(^{18}\text{O})$ of O_2 and $\delta(^{40}\text{Ar})$ for the period May 2012 – March 2020. The relationships of $\delta(\text{Ar}/\text{N}_2)$, $\delta(^{18}\text{O})$ and $\delta(^{40}\text{Ar})$ with $\delta(^{15}\text{N})$ indicate a significant artificial fractionation due to thermal diffusion during the air sample collection.

The $\delta_{\text{cor.}}(\text{O}_2/\text{N}_2)$ values, corrected for the artificial fractionation by using $\delta(\text{Ar}/\text{N}_2)$, and the $\delta(\text{APO})$ values derived from $\delta_{\text{cor.}}(\text{O}_2/\text{N}_2)$ were shown to have clear seasonal cycles nearly in opposite phase to that of the CO_2 amount fraction from the surface to 6 km along the latitudinal path from 25.5 to 33.5° N. We then used a three-dimensional atmospheric transport model NICAM-TM that was driven by the air-sea fluxes of O_2 , N_2 and CO_2 , along with fluxes of CO_2 and O_2 from fossil fuel combustion, to interpret some of the characteristic features we observed in the seasonal cycles and vertical profiles of APO and CO_2 amount fraction.

Seasonal amplitudes of $\delta(\text{APO})$ and CO_2 amount fraction decreased toward the lower latitude from 34.5 to 24.5° N by about 50% and less than 10%, respectively: these features were reproduced by the corresponding ratios from the control run of NICAM-TM. On the other hand, the w/o SH flux run underestimated the latitudinal change in the $\delta(\text{APO})$ amplitude, which indicated that the seasonal cycle of the mid-tropospheric $\delta(\text{APO})$ was modified significantly by a superposition of the northern and southern hemispheric seasonal cycles through the inter-hemispheric atmospheric mixing. The decrease in the $\delta(\text{APO})$



seasonal amplitude was about 70% with height from the surface to 6 km, while that of CO₂ amount fraction was less than 20%. These features were also reproduced well by the control run of NICAM-TM.

345 The observed decrease in the annual mean values of CO₂ amount fraction with height was reproduced by the control run of NICAM-TM. On the other hand, the average vertical gradient of the $\delta(\text{APO})$ profiles was slightly overestimated by the NICAM-TM simulations, while the simulated interannual variation was underestimated. This may be due to the ignored contribution of $\delta^{\text{AM}}(\text{APO})$, which is a component of $\delta(\text{APO})$ driven by annual mean air-sea O₂ and N₂ fluxes.

The interannual variations in the middle tropospheric $\delta^{\text{AM}}(\text{APO})$ were estimated by subtracting the simulated $\delta(\text{APO})$ by the NICAM-TM control run from the observed $\delta(\text{APO})$. We also estimated the solubility-driven component of $\delta(\text{APO})$ ($\delta_{\text{therm}}(\text{APO})$) from the $\delta(\text{Ar/N}_2)$ observed at Tsukuba, assuming its interannual variation was driven by changes in the globally-averaged solubility of the seawater. The interannual variation in $\delta(\text{APO})$ driven by marine biological activities ($\delta_{\text{netbio}}(\text{APO})$) was calculated by subtracting $\delta_{\text{therm}}(\text{APO})$ from $\delta^{\text{AM}}(\text{APO})$. The $\delta_{\text{netbio}}(\text{APO})$ showed significant interannual variations in the opposite phase to that of $\delta_{\text{therm}}(\text{APO})$, and the change rate varied in opposite phase with the NINO.WEST. Therefore, the
355 $\delta_{\text{netbio}}(\text{APO})$ values obtained in this study tended to increase and decrease with El Niño and La Niña, respectively, and is in agreement with Eddebber et al. (2017) who examined responses of the global and tropical air-sea O₂ flux to ENSO based on CESM.

By assuming the observed secular trends of the middle tropospheric $\delta_{\text{cor.}}(\text{O}_2/\text{N}_2)$ and CO₂ amount fraction to be representative of global average values, we estimated terrestrial biospheric and oceanic CO₂ uptakes to be (1.8±0.9) and
360 (2.8±0.6) Pg a⁻¹, respectively, for the period 2012-2019. These values agree well with the corresponding CO₂ uptake values of (1.8±1.1) (land) and (2.6±0.5) Pg a⁻¹ (ocean) reported by the GCP.

Additionally, our study has shown that our aircraft observation and the method we used to correct artificial fractionation of O₂ and N₂ are useful in evaluating inter-hemispheric air mixing processes based on the seasonal $\delta(\text{APO})$ cycle, as well as interannual variations in the global air-sea O₂ flux, and in calculating global CO₂ budgets based on the long-term trends of
365 $\delta_{\text{cor.}}(\text{O}_2/\text{N}_2)$ and CO₂ amount fraction.

Data availability.

The observational data of $\delta_{\text{cor.}}(\text{O}_2/\text{N}_2)$ and CO₂ amount fraction are available through the World Data Centre for Greenhouse Gases (WDCGG) at <https://gaw.kishou.go.jp>, and the respective DOIs are https://doi.org/10.50849/WDCGG_0006-8002-7001-05-02-9999 and https://doi.org/10.50849/WDCGG_0001-8002-1001-05-02-9999.
370

Author contributions.

SI designed the study, carried out measurements of $\delta(\text{O}_2/\text{N}_2)$, $\delta(\text{Ar/N}_2)$, $\delta^{15}\text{N}$, $\delta^{18}\text{O}$ and $\delta^{40}\text{Ar}$ and drafted the manuscript. KT, SK managed the collections, YN carried out the simulations of NICAM-TM using the supercomputer system (NEC SX-



375 Aurora Tsubasa) of the National Institute for Environmental Studies (NIES). HM, SM and KI examined the results and provide feedback on the manuscript. All the authors approved the final manuscript.

Competing interests.

The authors declare that they have no conflict of interest.

380

Acknowledgements.

The authors gratefully acknowledge many staff members of the Japan Ministry of Defense and Japan Meteorological Agency for supporting the long-term observation.

385 **Financial support.**

This study was partly supported by the JSPS KAKENHI (grant nos. 15H02814 and 19H01975) and the Global Environment Research Coordination System from the Ministry of the Environment, Japan (grant nos. METI1454 and METI1953).

References

- 390 Andres, R. J., Boden, T., and Marland, G.: Monthly Fossil-Fuel CO₂ Emissions: Mass of Emissions Gridded by One Degree Latitude by One Degree Longitude, Carbon Dioxide Information Analysis Center, Oak Ridge National Laboratory, U.S. Department of Energy, Oak Ridge, Tenn., U.S.A., <https://doi.org/10.3334/CDIAC/ffe.MonthlyMass.2016>, 2016.
- Aoki, N., Ishidoya, S., Matsumoto, N., Watanabe, T., Shimosaka, T., and Murayama, S.: Preparation of primary standard mixtures for atmospheric oxygen measurements with less than 1 μmol mol⁻¹ uncertainty for oxygen molar fractions, Atmos. Meas. Tech., 12, 2631–2646, <https://doi.org/10.5194/amt-12-2631-2019>, 2019.
- 395 Bender, M. L., Ho, D. T., Hendricks, M. B., Mika, R., Battle, M. and co-authors.: Atmospheric O₂/N₂ changes, 1993-2002: Implications for the partitioning of fossil fuel CO₂ sequestration. Global Biogeochem. Cycles. 19, GB4017, doi:10.1029/2004GB002410, 2005.
- Birner, B., Chipperfield, M. P., Morgan, E. J., Stephens, B. B., Linz, M., Feng, W., Wilson, C., Bent, J. D., Wofsy, S. C., Severinghaus, J., and Keeling, R. F.: Gravitational separation of Ar/N₂ and age of air in the lowermost stratosphere in airborne observations and a chemical transport model, Atmos. Chem. Phys., 20, 12391–12408, <https://doi.org/10.5194/acp-20-12391-2020>, 2020.
- 400 Bopp, L., Le Quéré, C., Heimann, M., Manning, A. C., and Monfray, P.: Climate-induced oceanic oxygen fluxes: implications for the contemporary carbon budget, Global Biogeochem. Cy., 16, 1022, <https://doi.org/10.1029/2001GB001445>, 2002.
- 405 Blaine, T. W.: Continuous measurements of atmospheric argon/ nitrogen as a tracer of air-sea heat flux: Models, methods, and data. Ph.D. thesis, Univ. of Calif., San Diego, La Jolla, 2005.



- Eddebbbar, Y. A., Long, M. C., Resplandy, L., Rödenbeck, C., Rodgers, K. B., Manizza, M., and Keeling, R. F.: Impacts of ENSO on air-sea oxygen exchange: Observations and mechanisms, *Global Biogeochem. Cy.*, **31**, 901–921, <https://doi.org/10.1002/2017GB005630>, 2017.
- 410 Garcia, H., and Keeling, R.: On the global oxygen anomaly and air-sea flux, *J. Geophys. Res.* **106** (C12), 31155–31166, 2001.
- Gilfillan, D., Marland, G., Boden, T., and Andres, R.: Global, Regional, and National Fossil-Fuel CO₂ Emissions, Carbon Dioxide Information Analysis Center at Appalachian State University, Boone North Carolina, available at: <https://energy.appstate.edu/CDIAC>, 2019
- Friedlingstein, P., O'Sullivan, M., Jones, M. W., Andrew, R. M., Hauck, J., Olsen, A., Peters, G. P., Peters, W., Pongratz, J., 415 Sitch, S., Le Quééré, C., Canadell, J. G., Ciais, P., Jackson, R. B., Alin, S., Aragão, L. E. O. C., Arneeth, A., Arora, V., Bates, N. R., Becker, M., Benoit-Cattin, A., Bittig, H. C., Bopp, L., Bultan, S., Chandra, N., Chevallier, F., Chini, L. P., Evans, W., Florentie, L., Forster, P. M., Gasser, T., Gehlen, M., Gilfillan, D., Gkritzalis, T., Gregor, L., Gruber, N., Harris, I., Hartung, K., Haverd, V., Houghton, R. A., Ilyina, T., Jain, A. K., Joetzjer, E., Kadono, K., Kato, E., Kitidis, V., Korsbakken, J. I., Landschützer, P., Lefèvre, N., Lenton, A., Lienert, S., Liu, Z., Lombardozi, D., Marland, G., Metzl, 420 N., Munro, D. R., Nabel, J. E. M. S., Nakaoka, S.-I., Niwa, Y., O'Brien, K., Ono, T., Palmer, P. I., Pierrot, D., Poulter, B., Resplandy, L., Robertson, E., Rödenbeck, C., Schwinger, J., Séférian, R., Skjelvan, I., Smith, A. J. P., Sutton, A. J., Tanhua, T., Tans, P. P., Tian, H., Tilbrook, B., van der Werf, G., Vuichard, N., Walker, A. P., Wanninkhof, R., Watson, A. J., Willis, D., Wiltshire, A. J., Yuan, W., Yue, X., and Zaehle, S.: Global Carbon Budget 2020, *Earth Syst. Sci. Data*, **12**, 3269–3340, <https://doi.org/10.5194/essd-12-3269-2020>, 2020.
- 425 Goto, D., Morimoto, S., Ishidoaya, S., Aoki, S. and Nakazawa, T.: Terrestrial biospheric and oceanic CO₂ uptake estimated from long-term measurements of atmospheric CO₂ mole fraction, $\delta^{13}\text{C}$ and $\delta(\text{O}_2/\text{N}_2)$ at Ny-Ålesund, Svalbard. *J. Geophys. Res. Biogeosci.*, **122**, doi:10.1002/2017JG003845, 2017.
- Ishidoaya, S., Morimoto, S., Sugawara, S., Watai, T., Machida, T. Aoki, S., Nakazawa, T., and Yamanouchi, T.: Gravitational separation suggested by O₂/N₂, $\delta^{15}\text{N}$ of N₂, $\delta^{18}\text{O}$ of O₂, Ar/N₂ observed in the lowermost part of the stratosphere at northern 430 middle and high latitudes in the early spring of 2002, *Geophys. Res. Lett.*, **35**, L03812, doi:10.1029/2007GL031526, 2008.
- Ishidoaya, S., Aoki, S., Goto, D., Nakazawa, T., Taguchi, S. and co-authors. 2012. Time and space variations of the O₂/N₂ ratio in the troposphere over Japan and estimation of global CO₂ budget. *Tellus B.* **64**, 18964, <http://dx.doi.org/10.3402/tellusb.v64i0.18964>.
- Ishidoaya, S., Sugawara, S., Morimoto, S., Aoki, S., Nakazawa, T. and co-authors. 2013b. Gravitational separation in the 435 stratosphere – a new indicator of atmospheric circulation. *Atmos. Chem. Phys.* **13**, 8787–8796, 2013, www.atmos-chem-phys.net/13/8787/2013/, doi:10.5194/acp-13-8787-2013.
- Ishidoaya, S., and Murayama, S.: Development of high precision continuous measuring system of the atmospheric O₂/N₂ and Ar/N₂ ratios and its application to the observation in Tsukuba, Japan, *Tellus B.* **66**, 22574, <http://dx.doi.org/10.3402/tellusb.v66.22574>, 2014.



- 440 Ishidoya, S., Tsuboi, K., Matsueda, H., Murayama, S., Taguchi, S. and co-authors. 2014. New atmospheric O₂/N₂ ratio measurements over the western North Pacific using a cargo aircraft C-130H. *SOLA*. **10**, 23-28, doi:10.2151/sola.2014-006.
- Ishidoya, S., Tsuboi, K., Murayama, S., Matsueda, H., Aoki, N., Shimosaka, T., Kondo, H., and Saito, K.: Development of a continuous measurement system for atmospheric O₂/N₂ ratio using a paramagnetic analyzer and its application in
445 Minamitorishima Island, Japan, *SOLA*, 13, 230-234, 2017.
- Ishidoya, S., Sugawara, S., Tohjima, Y., Goto, D., Ishijima, K., Niwa, Y., Aoki, N., and Murayama, S.: Secular change in atmospheric Ar/N₂ and its implications for ocean heat uptake and Brewer–Dobson circulation, *Atmos. Chem. Phys.*, 21, 1357– 1373, <https://doi.org/10.5194/acp-21-1357-2021>, 2021.
- IUPAC Green Book, 3rd edition, prepared for publication by E.R. Cohen, T. Cvitas, J.G. Frey, B. Holmstrom, K. Kuchitsu, R.
450 Marquardt, I. Mills, F. Pavese, M. Quack, J. Stohner, H. Strauss, M. Takami, and A.J. Thor, RSC Publishing, 2007.
- Kawamura, K., Severinghaus, J., Ishidoya, S., Sugawara, S., Hashida, G., Motoyama, H., Fujii, Y., Aoki, S., and Nakazawa, T.: Convective mixing of air in firm at four polar sites, *Earth and Planetary Science Letters*, 244, 672-682., 2006.
- Keeling, R. F.: Development of an interferometric oxygen analyzer for precise measurement of the atmospheric O₂ mole fraction, *Ph.D. thesis*, Harvard University, Cambridge, 1988.
- 455 Keeling, R. F. and Shertz, S. R. 1992. Seasonal and interannual variations in atmospheric oxygen and implications for the global carbon cycle, *Nature*. **358**, 723-727.
- Keeling, R. F., Bender, M. L., and Tans, P. P.: What atmospheric oxygen measurements can tell us about the global carbon cycle, *Global Biogeochem. Cycles*, 7, 37-67, 1993.
- Keeling, R. F., Stephens, B. B., Najjar, R. G., Doney, S. C., Archer, D., and Heimann, M.: Seasonal variations in the
460 atmospheric O₂/N₂ ratio in relation to the kinetics of air-sea gas exchange. *Global Biogeochem. Cycles*. 12, 141-163, 1998.
- Keeling, R. F., Körtzinger, A., and Gruber, N.: Ocean deoxygenation in a warming world, *Annu. Rev. Marin. Sci.*, 2, 199-229, doi:10.1146/annurev.marine.010908.163855, 2010.
- Keeling, R. F. and Manning, A. C.: Studies of recent changes in atmospheric O₂ content, in *Treatise on Geochemistry*, vol. 5,
465 2nd ed., Elsevier, Amsterdam, 385–404, 2014.
- Kobayashi, S., Ota, Y., Harada, Y., Ebita, A., Moriya, M., On-oda, H., Onogi, K., Kamahori, H., Kobayashi, C., Endo, H., Miyaoka, K., and Takahashi, K.: The JRA-55 Reanalysis: general specifications and basic characteristics, *J. Meteorol. Soc. Jpn.*, 93, 5–48, <https://doi.org/10.2151/jmsj.2015-001>, 2015.
- Le Quéré, C., Andrew, R. M., Friedlingstein, P., Sitch, S., Hauck, J., Pongratz, J., Pickers, P. A., Korsbakken, J. I., Peters, G.
470 P., Canadell, J. G., Arneeth, A., Arora, V. K., Barbero, L., Bastos, A., Bopp, L., Chevallier, F., Chini, L. P., Ciais, P., Doney, S. C., Gkritzalis, T., Goll, D. S., Harris, I., Haverd, V., Hoffman, F. M., Hoppema, M., Houghton, R. A., Hurtt, G., Ilyina, T., Jain, A. K., Johannessen, T., Jones, C. D., Kato, E., Keeling, R. F., Gold-ewijk, K. K., Landschützer, P., Lefèvre, N., Lienert, S., Liu, Z., Lombardozi, D., Metzl, N., Munro, D. R., Nabel, J. E. M. S., Nakaoka, S.-I., Neill, C.,



- 475 Olsen, A., Ono, T., Patra, P., Peregón, A., Peters, W., Peylin, P., Pfeil, B., Pierrot, D., Poulter, B., Re- hder, G., Resplandy, L., Robertson, E., Rocher, M., Rödenbeck, C., Schuster, U., Schwinger, J., Séférian, R., Skjelvan, I., Stein- hoff, T., Sutton, A., Tans, P. P., Tian, H., Tilbrook, B., Tubiello, F. N., van der Laan-Luijkx, I. T., van der Werf, G. R., Viovy, N., Walker, A. P., Wiltshire, A. J., Wright, R., Zaehle, S., and Zheng, B.: Global Carbon Budget 2018, *Earth Syst. Sci. Data*, 10, 2141– 2194, <https://doi.org/10.5194/essd-10-2141-2018>, 2018.
- 480 Levitus, S., Antonov, J. I., Boyer, T. P., Baranova, O. K., Garcia, H. E., Locarnini, R. A., Mishonov, A. V., Reagan, J. R., Seidov, D., Yarosh, E. S., and Zweng, M. M.: World ocean heat content and thermosteric sea level change (0–2000 m), 1955–2010, *Geophys. Res. Lett.*, 39, L10603, <https://doi.org/10.1029/2012GL051106>, 2012.
- Manning, A. C. and Keeling, R. F.: Global oceanic and terrestrial biospheric carbon sinks from the Scripps atmospheric oxygen flask sampling network. *Tellus B*. 58, 95– 116, 2006.
- 485 McKinley, G. A., Follows, M. J., Marchall, J., and Fan, S.-M.: Inter- annual variability of air-sea O₂ fluxes and the determination of CO₂ sinks using atmospheric O₂/N₂, *Geophys. Res. Lett.*, 30(3), 1101, doi:10.1029/2002GL016044 ,2003.
- Morgan, E. J., Stephens, B. B., Long, M. C., Keeling, R. F., Bent, J. D., McKain, K., Sweeney, C., Hoecker- Martínez, M. S., and Kort, E. A.: Summertime Atmo- spheric Boundary Layer Gradients of O₂ and CO₂ over the Southern Ocean, *J. Geophys. Res.*, 124, 13439–13456, <https://doi.org/10.1029/2019JD031479>, 2019.
- 490 Nakazawa, T., Ishizawa, M., Higuchi, K., and Trivett, N. B. A.: Two curve fitting methods applied to CO₂ flask data. *Environmetrics*. 8, 197-218, 1997a.
- Nakazawa, T., Morimoto, S., Aoki, S. and Tanaka, M.: Temporal and spatial variations of the carbon isotopic ratio of atmospheric carbon dioxide in the western Pacific region, *J. Geophys. Res.*, 102, 1271-1285, 1997b.
- 495 Nevison, C. D., Keeling, R. F., Kahru, M., Manizza, M., Mitchell, B. G., Cassar N.: Estimating net community production in the Southern ocean based on atmospheric potential oxygen and satellite ocean color data, *Glob. Biogeochem. Cycles.*, 26, GB1020. DOI: <http://dx.doi.org/10.1029/2011GB004040>, 2012.
- Niwa, Y., Tomita, H., Satoh, M., and Imasu, R.: A Three-Dimensional Icosahedral Grid Advection Scheme Preserving Monotonicity and Consistency with Continuity for Atmospheric Tracer Transport, *J. Meteorol. Soc. Jpn.*, 89, 255–268, doi:10.2151/jmsj.2011-306, 2011.
- 500 Niwa, Y., Machida, T., Sawa, Y., Matsueda, H., Schuck, T. J., Brenninkmeijer, C. A. M., Imasu, R., and Satoh, M.: Imposing strong constraints on tropical terrestrial CO₂ fluxes using passenger aircraft based measurements, *J. Geophys. Res.*, 117, doi:10.1029/2012JD017474, 2012.
- 505 Niwa, Y., Tsuboi, K., Matsueda, H., Sawa, Y., Machida, T., Nakamura, M., Kawasato, T., Saito, K., Takatsuji, S., Tsuji, K., Nishi, H., Dehara, K., Baba, Y., Kuboike, D., Iwatsubo, S., Ohmori, H., and Hanamiya, Y.: Seasonal Variations of CO₂, CH₄, N₂O and CO in the Mid-troposphere over the Western North Pacific Observed using a C-130H Cargo Aircraft, *J. Meteorol. Soc. Japan*, 92(1), doi:10.2151/jmsj.2014-104, 2014.



- Rödenbeck, C., Le Quéré, C., Heimann, M., and Keeling, R. F.: Interannual variability in oceanic biogeochemical processes inferred by inversion of atmospheric O₂/N₂ and CO₂ data, *Tellus B*, **60**, 685–705, <https://doi.org/10.1111/j.1600-0889.2008.00375.x>, 2008.
- 510 Satoh, M., Matsuno, T., Tomita, H., Miura, H., Nasuno, T., and Iga, S.: Nonhydrostatic icosahedral atmospheric model (NICAM) for global cloud resolving simulations, *J. Comput. Phys.*, **227**, 3486–3514, doi:10.1016/j.jcp.2007.02.006, 2008.
- Satoh, M., Tomita, H., Yashiro, H., Miura, H., Kodama, C., Seiki, T., Noda, A. T., Yamada, Y., Goto, D., Sawada, M., Miyoshi, T., Niwa, Y., Hara, M., Ohno, T., Iga, S., Arakawa, T., Inoue, T., and Kubokawa, H.: The Non-hydrostatic Icosahedral Atmospheric Model: description and development, *Progress in Earth and Planetary Science*, **1**, 1–32, doi:10.1186/s40645-014-0018-1, 2014.
- 515 Severinghaus, J.: Studies of the terrestrial O₂ and carbon cycles in sand dune gases and in biosphere 2, *Ph. D. thesis, Columbia University*, New York, 1995.
- Stephens, B. B., Keeling, R. F., Heimann, M., Six, K., Murnane, R. and co-authors.: Testing global ocean carbon cycle models using measurements of atmospheric O₂ and CO₂ concentration. *Global Biogeochem. Cycles* **12** (2), 213-230, 1998.
- 520 Stephens, B. B., Keeling, R. F. and Paplawsky, W. J. 2003. Shipboard measurements of atmospheric oxygen using a vacuum-ultraviolet absorption technique. *Tellus B*. **55**, 857–878.
- Stephens, B. B., Morgan, E. J., Bent, J. D., Keeling, R. F., Watt, A. S., Shertz, S. R., and Daube, B. C.: Airborne measurements of oxygen concentration from the surface to the lower stratosphere and pole to pole, *Atmos. Meas. Tech.*, **14**, 2543–2574, <https://doi.org/10.5194/amt-14-2543-2021>, 2021.
- 525 Sturm, P., Leuenberger, M., Moncrieff, J. and Ramonet, M. 2005. Atmospheric O₂, CO₂ and δ¹³C measurements from aircraft sampling over Griffin Forest, Perthshire, UK. *Rapid Commun. Mass Spectrom.* **19**, 2399-2406, doi:10.1002/rcm.2071.
- Takahashi, T., Sutherland, S. C., Wanninkhof, R., Sweeney, C., Feely, R. A., Chipman, D. W., Hales, B., Friederich, G., Chavez, F., Sabine, C., Watson, A., Bakker, D. C. E., Schuster, U., Metzl, N., Yoshikawa-Inoue, H., Ishii, M., Midorikawa, T., Nojiri, Y., Körtzinger, A., Steinhoff, T., Hoppema, M., Olafsson, J., Arnarson, T. S., Tilbrook, B., Johannessen, T., Olsen, A., Bellerby, R., Wong, C. S., Delille, B., Bates, N. R., and de Baar, H. J. W.: Climatological mean and decadal change in surface ocean pCO₂, and net sea-air CO₂ flux over the global oceans, *Deep Sea Res. Pt. II*, **56**, 554–577, <https://doi.org/10.1016/j.dsr2.2008.12.009>, 2009.
- 530 Tohjima, Y., Mukai, H., Nojiri, Y., Yamagishi, H. and Machida, T.: Atmospheric O₂/N₂ measurements at two Japanese sites: estimation of global oceanic and land biotic carbon sinks and analysis of the variations in atmospheric potential oxygen (APO). *Tellus B*. **60**, 213-225, 2008.
- Tohjima, Y., Minejima, C., Mukai, H., Machida, T., Yamagishi, H., and Nojiri, Y.: Analysis of seasonality and annual mean distribution of atmospheric potential oxygen (APO) in the Pacific region, *Glob. Biogeochem. Cy.*, **26**, GB4008, <https://doi.org/10.1029/2011GB004110>, 2012.



- Tohjima, Y., Mukai, H., Machida, T., Hoshina, Y., and Nakaoka, S.-I.: Global carbon budgets estimated from atmospheric
540 O_2/N_2 and CO_2 observations in the western Pacific region over a 15-year period, *Atmos. Chem. Phys.*, 19, 9269–9285,
<https://doi.org/10.5194/acp-19-9269-2019>, 2019.
- Trenberth, K. E.: Seasonal variations in global sea level pressure and the total mass of the atmosphere, *J. Geophys. Res.*, 86,
5238– 5246, 1981.
- Tsuboi, K., Matsueda, H., Sawa, Y., Niwa, Y., Nakamura, M., Kuboike, D., K. Saito, K., Ohmori, H., Iwatsubo, S., Nishi, H.,
545 Hanamiya, Y., Tsuji, K., and Baba, Y.: Evaluation of a new JMA aircraft flask sampling system and laboratory trace gas
analysis system, *Atoms. Meas. Tech.*, 6, 1257–1270, doi: 10.5194/amt-6-1257-2013, 2013.
- Van der Laan, S., van der Laan-Luijk, I.T., Rödenbeck, C., Varlagin, A., Shironya, I. and Neubert, R.E.M, Ramonet, M.:
Atmospheric CO_2 , $\delta(O_2/N_2)$, APO and oxidative ratios from aircraft flask samples over Fyodorovskoye, Western Russia,
Atmos. Environ., 97, 174-181, 2014.
- 550 Weiss, R. F.: The solubility of nitrogen, oxygen and argon in water and seawater, *Deep-Sea Res.*, 17, 721–735, 1970.
- Wofsy et al.: HIAPER Pole-to-Pole Observations (HIPPO): fine grained, global-scale measurements of climatically important
atmospheric gases and aerosols, *Philos. T. Roy. Soc. A*, 369, 2073– 2086, <https://doi.org/10.1098/rsta.2010.0313>, 2011.



555

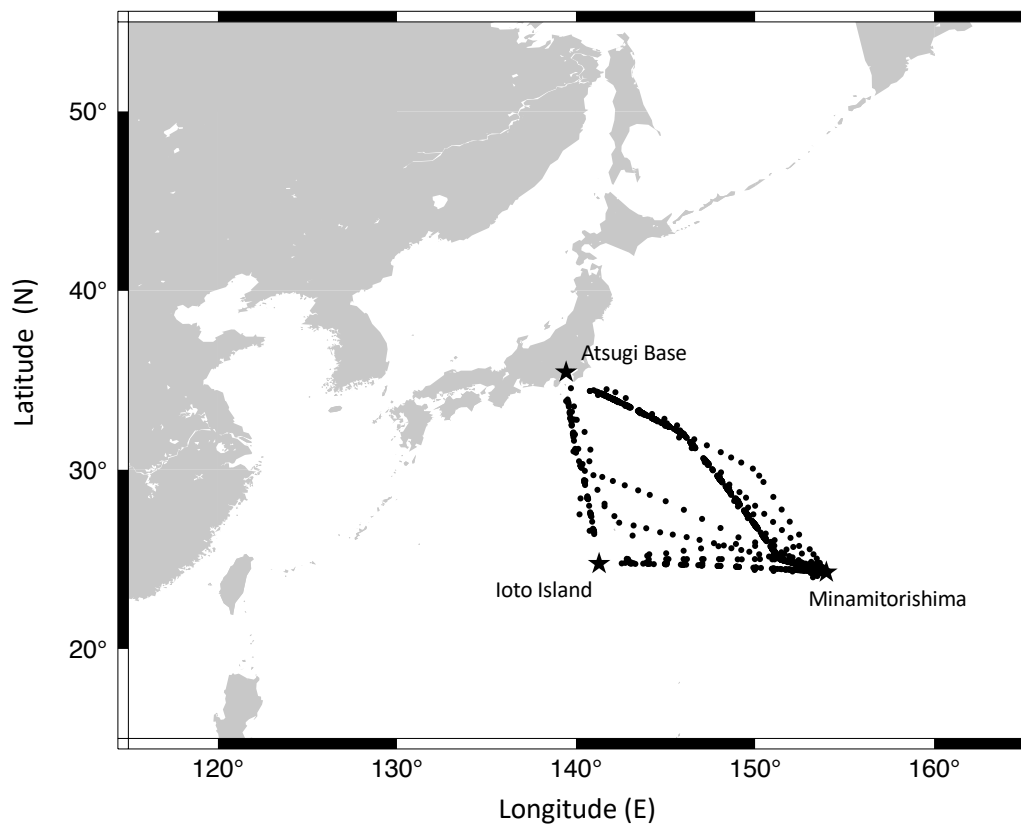
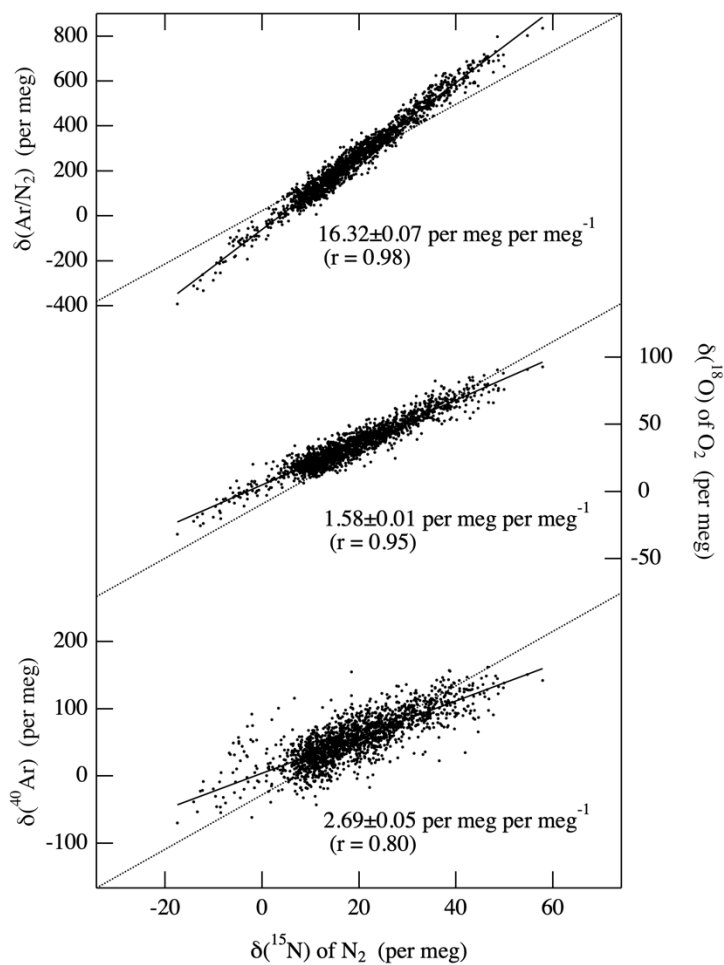


Figure 1: Locations of C-130 aircraft air sampling for the period May 2012 – March 2020 (circles). Locations of Minamitorishima (MNM), Ioto Island, and Atsugi Base are also shown by stars.

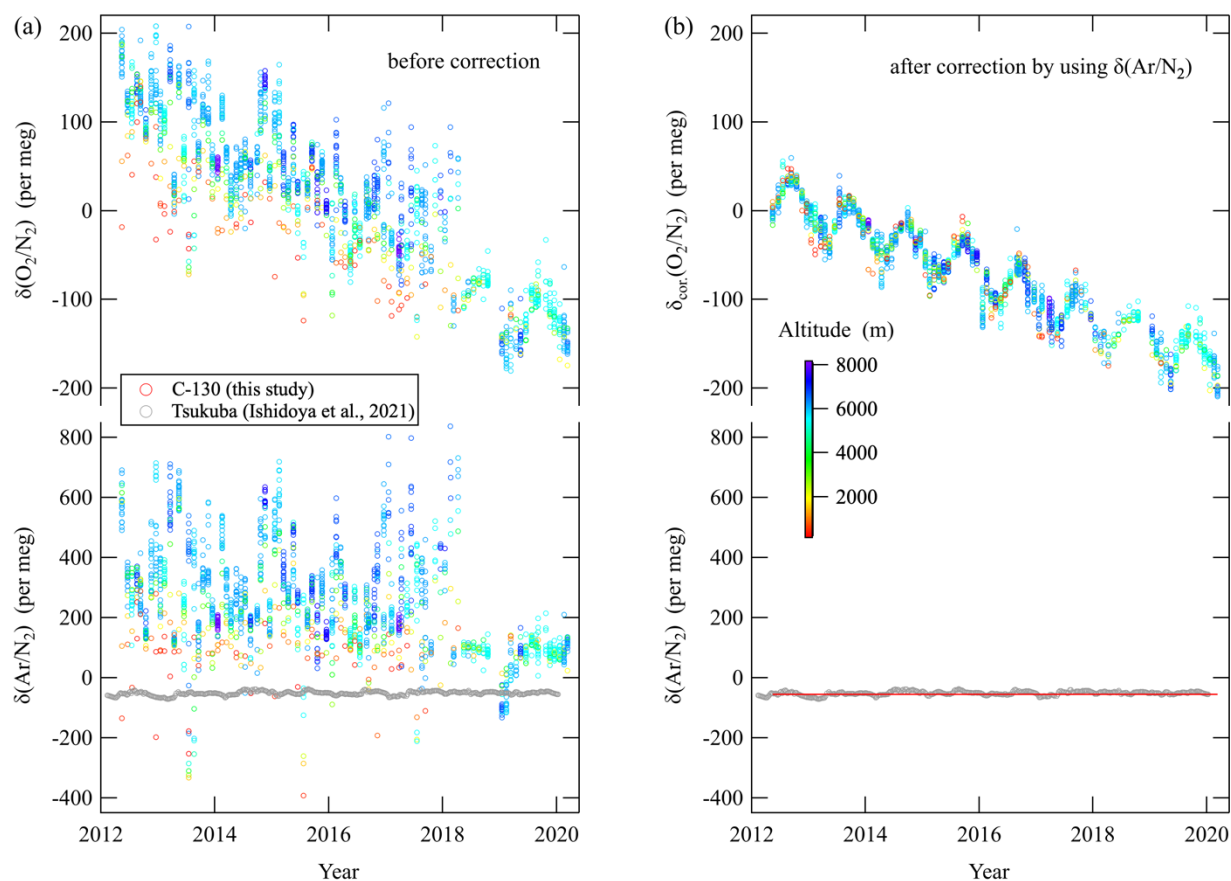
560



565 **Figure 2:** Measured $\delta(\text{Ar}/\text{N}_2)$, $\delta(^{18}\text{O})$ of O_2 and $\delta(^{40}\text{Ar})$ plotted against $\delta(^{15}\text{N})$ of N_2 for all the collected air samples (solid dots). Least-squares regression lines fitted to the data are shown as solid lines, while the relationships expected from mass-dependent fractionation of air molecules are shown by dotted lines.

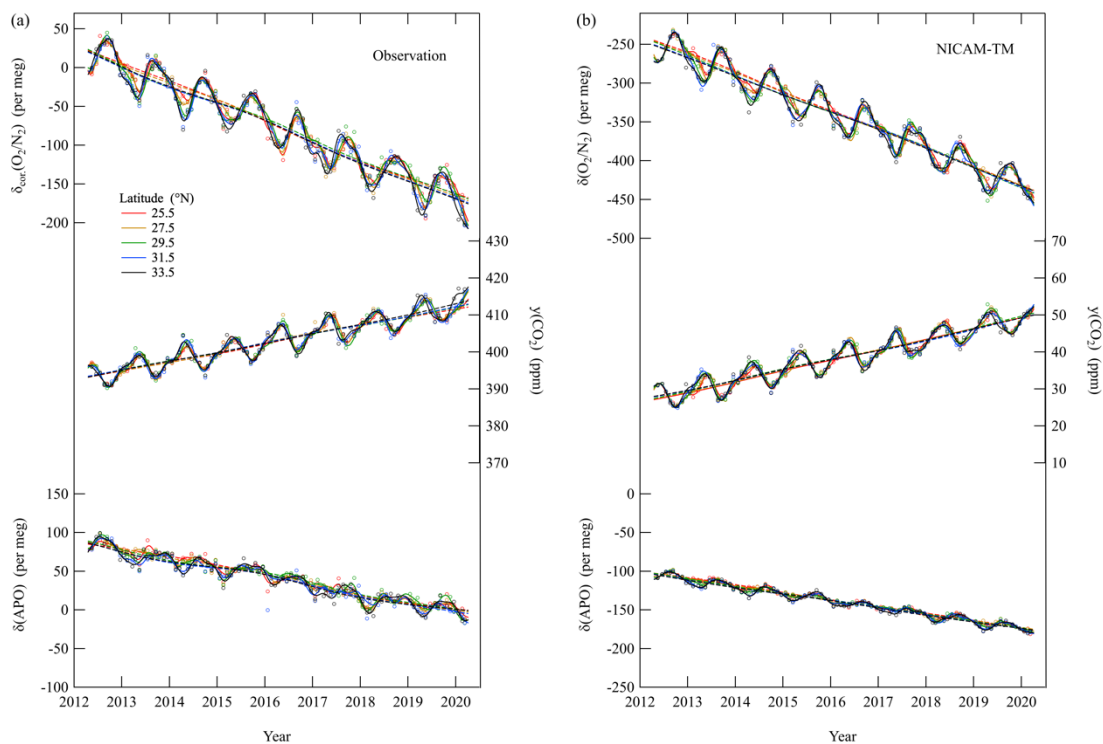


570



575

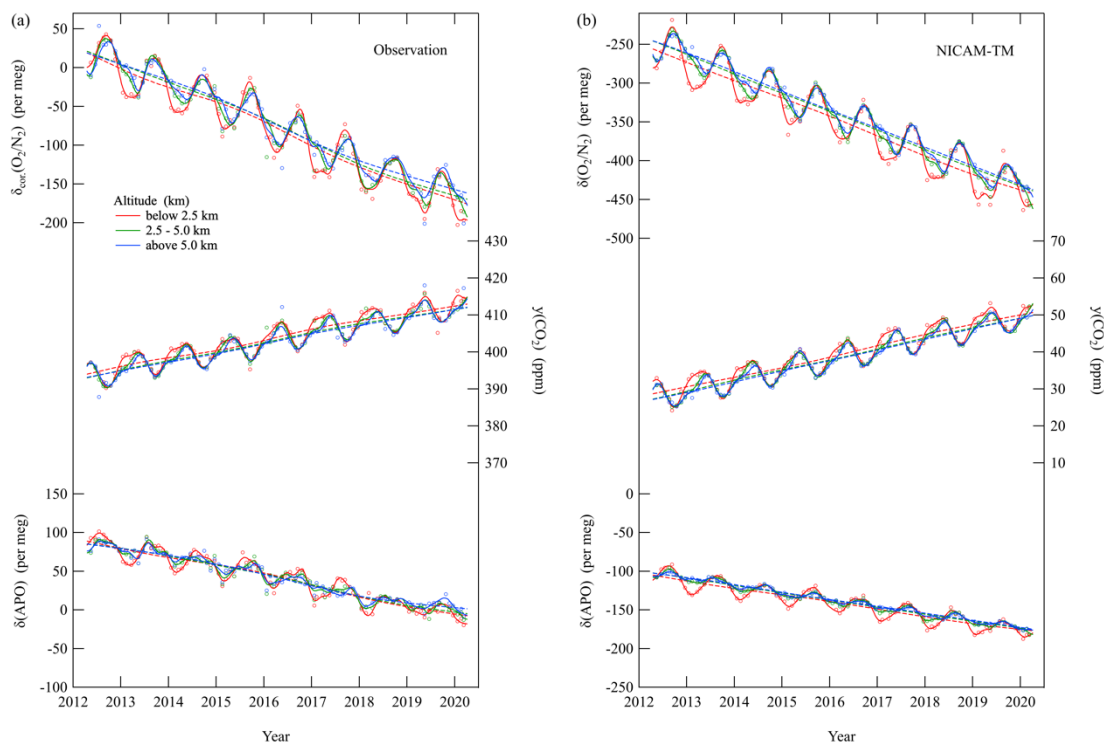
Figure 3: (a) Measured values of $\delta(\text{O}_2/\text{N}_2)$ and $\delta(\text{Ar}/\text{N}_2)$ for all the air samples collected onboard the C-130 aircraft. $\delta(\text{Ar}/\text{N}_2)$ values observed at Tsukuba, Japan are also shown as gray circles (Ishidoya et al., 2021). (b) Same as in (a) but for the $\delta_{\text{cor}}(\text{O}_2/\text{N}_2)$ corrected for artificial fractionation by applying eq. (6) (see text). $\delta(\text{Ar}/\text{N}_2)$ value for the reference point of eq. (6) are also shown by red line. Color bar indicates the altitude where the air sampling were carried out.



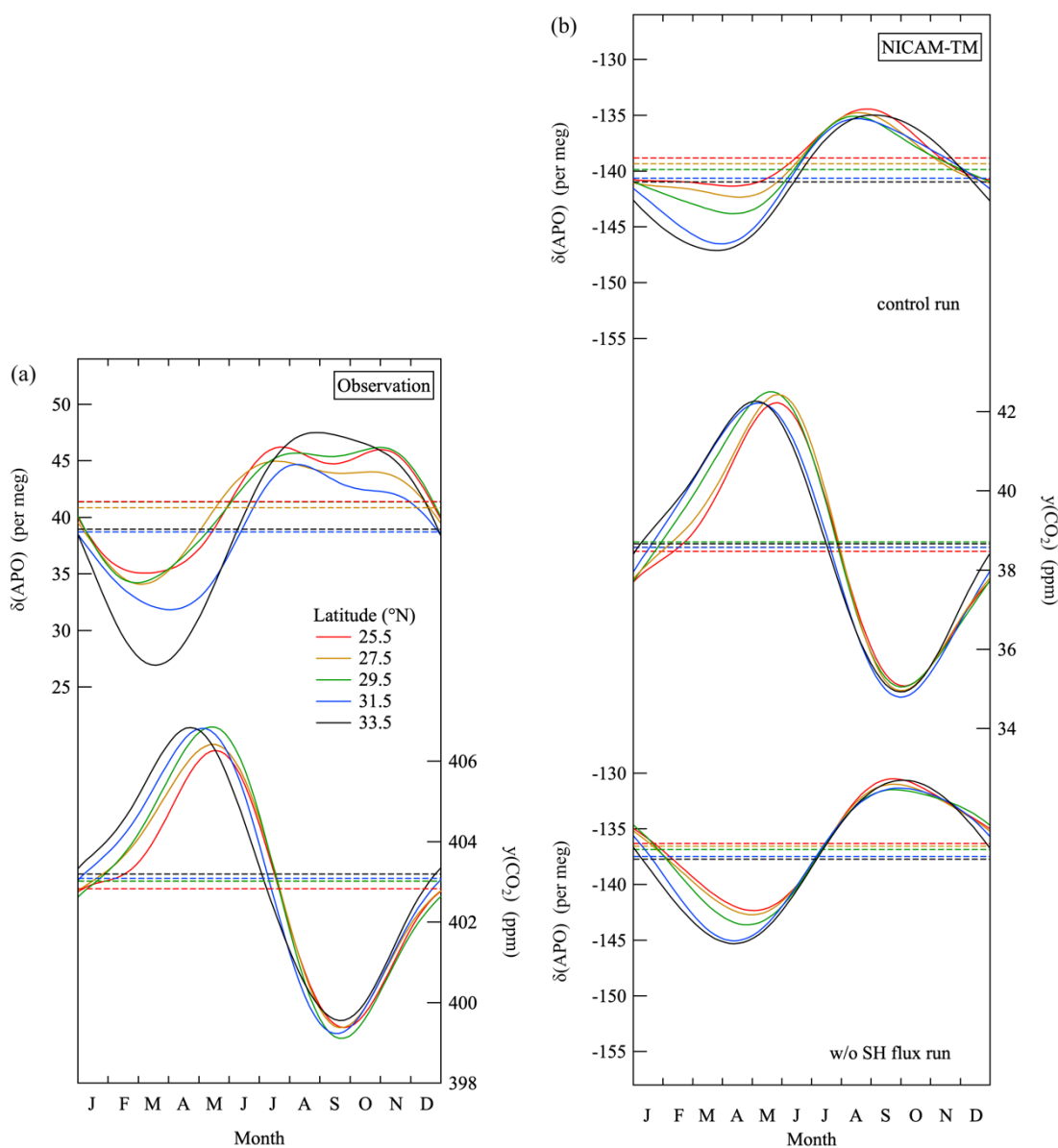
580

Figure 4: (a) $\delta_{\text{cor}}(\text{O}_2/\text{N}_2)$, CO_2 amount fraction and $\delta(\text{APO})$ observed at the height of (6.1 ± 0.5) ($\pm 1\sigma$) km at various latitudes over the western North Pacific. Best-fit curves to the data (solid lines) and secular trends (dashed lines) are also shown. (b) Same as in (a) but for calculated values obtained from the NICAM-TM control-run.

585



590 **Figure 5: (a) $\delta_{\text{cor.}}(\text{O}_2/\text{N}_2)$, CO_2 amount fraction and $\delta(\text{APO})$ observed in the troposphere over MNM. Best-fit curves to the data (solid lines) and secular trends (dashed lines) are also shown. (b) Same as in (a) but for calculated values using NICAM-TM.**



595

Figure 6: (a) Average seasonal cycles of $\delta(\text{APO})$ and CO_2 amount fraction observed in the troposphere at various latitudes over the western North Pacific. Dashed lines denote the average values throughout the observation period. (b) Same as in (a) but for calculated values obtained from the NICAM-TM control run and the corresponding results from the w/o SH flux run (see text).

600

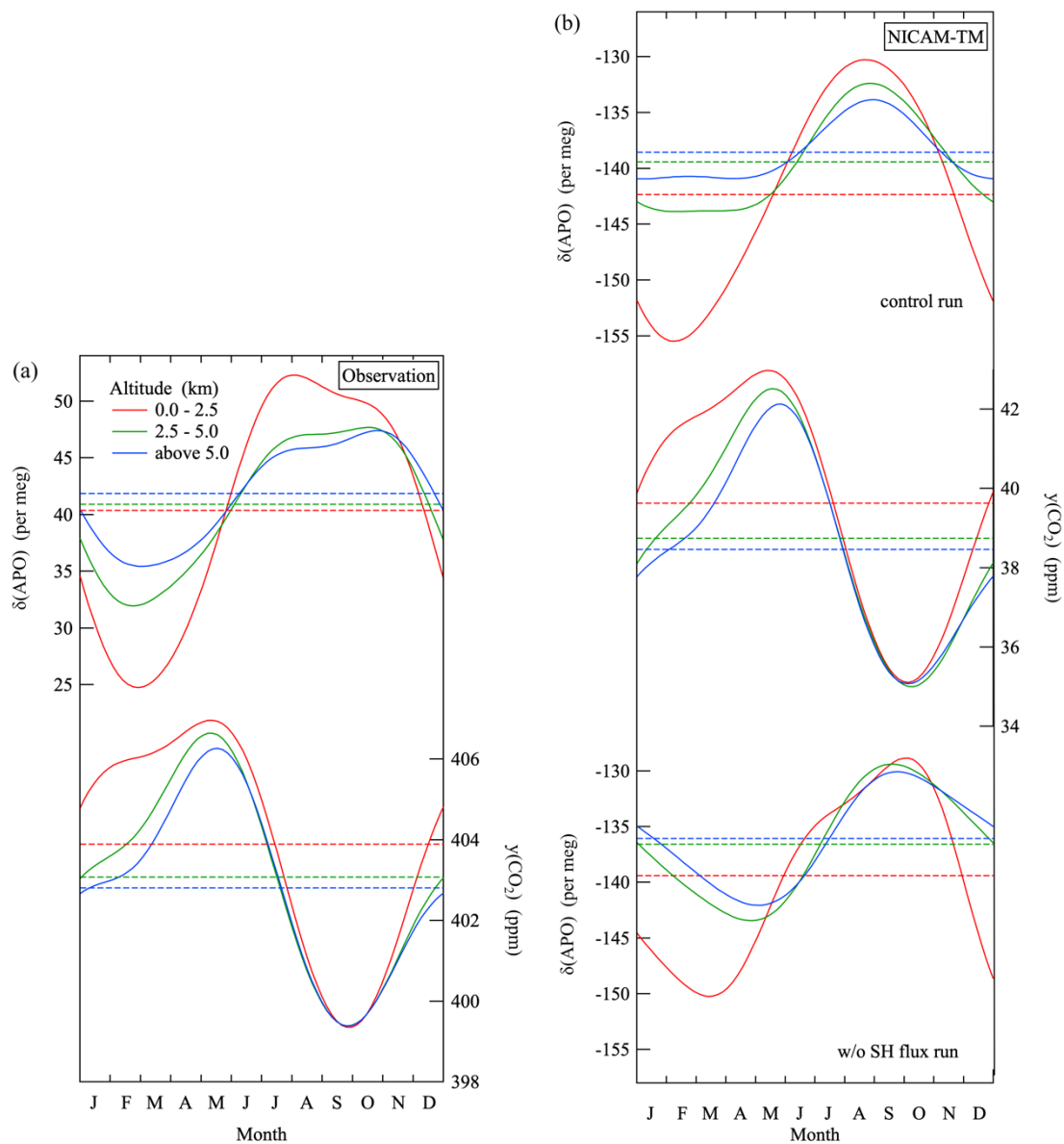
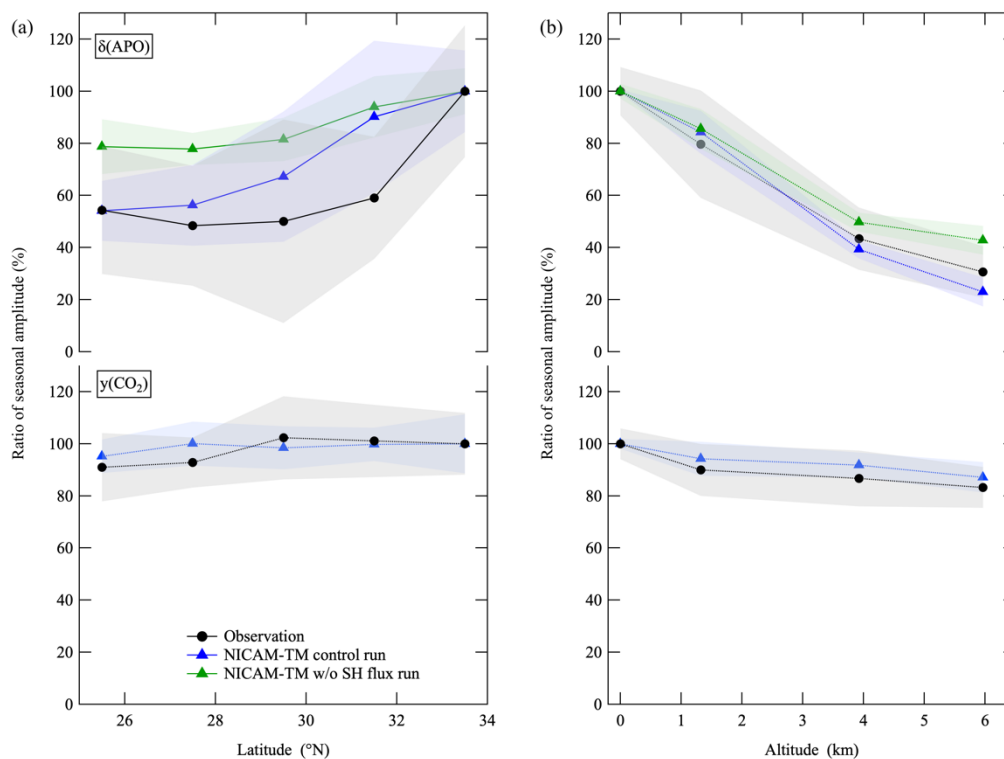
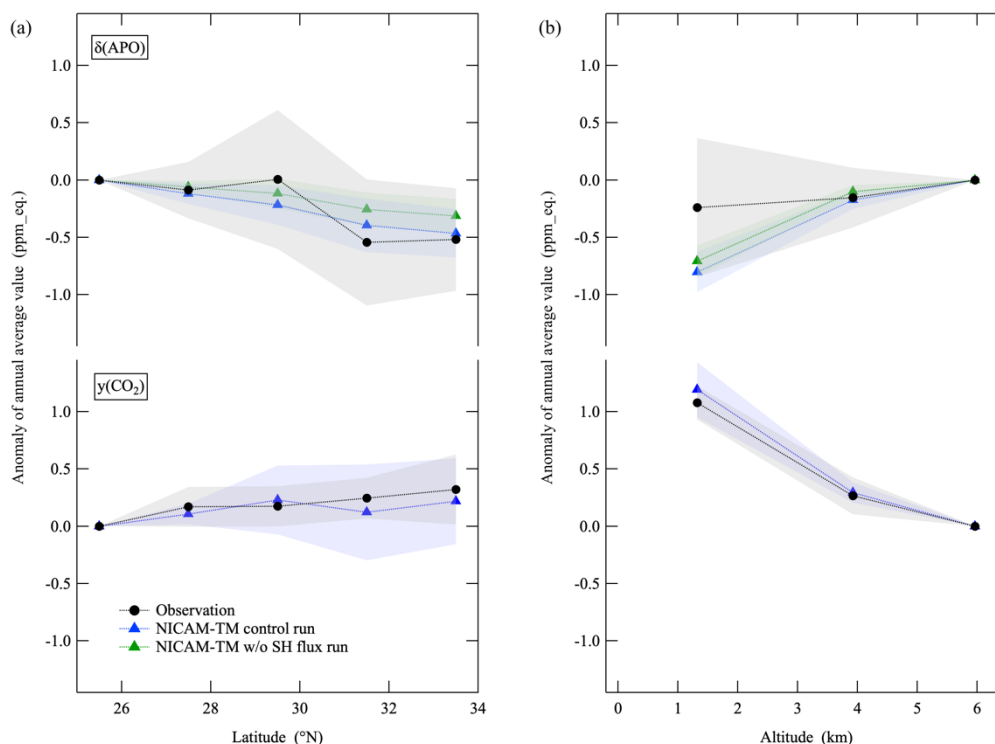


Figure 7: Same as in Fig. 6 but for those in the troposphere over MNM.



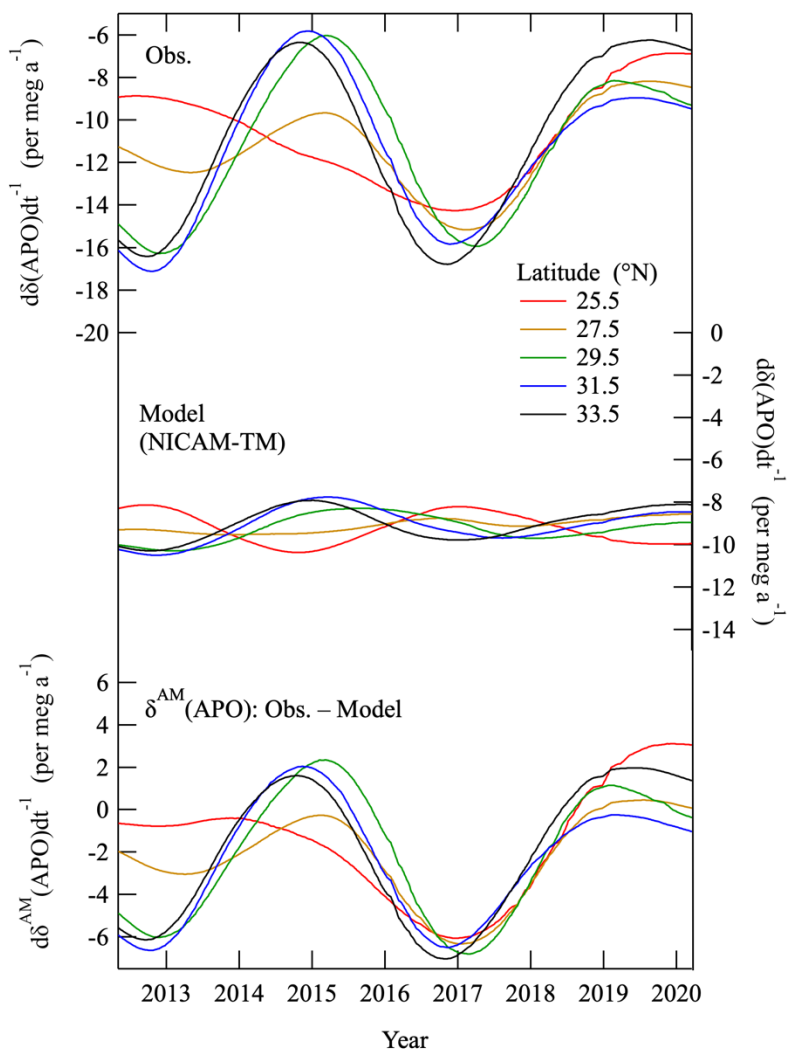
610 **Figure 8:** (a) Latitudinal distribution of average ratios of the observed seasonal $\delta(\text{APO})$ and CO_2 amount fraction amplitudes
 calculated relative to the values observed at 33.5°N in the troposphere over the western North Pacific throughout the observation
 period (black filled circles). Error bands (shaded) indicate year-to-year variations ($\pm 1\sigma$). The corresponding results calculated using
 NICAM-TM control run (blue triangles) and w/o SH flux run (green triangles) are also shown. (b) Same as in (a) but for vertical
 distribution over MNM relative to the corresponding values at 6 km.

615



620 **Figure 9:** (a) Latitudinal distribution of average deviations of the annual mean values of $\delta(\text{APO})$ and CO_2 amount fraction relative to those at 25.5° N in the troposphere over the western North Pacific throughout the observation period (black filled circles). Error bands (shaded) indicate year-to-year variations ($\pm 1\sigma$). The corresponding results calculated using NICAM-TM for control run (blue triangles) and w/o SH flux run (green triangles) are also shown. (b) Same as in (a) but for vertical distribution over MNM relative to the corresponding values at 6 km.

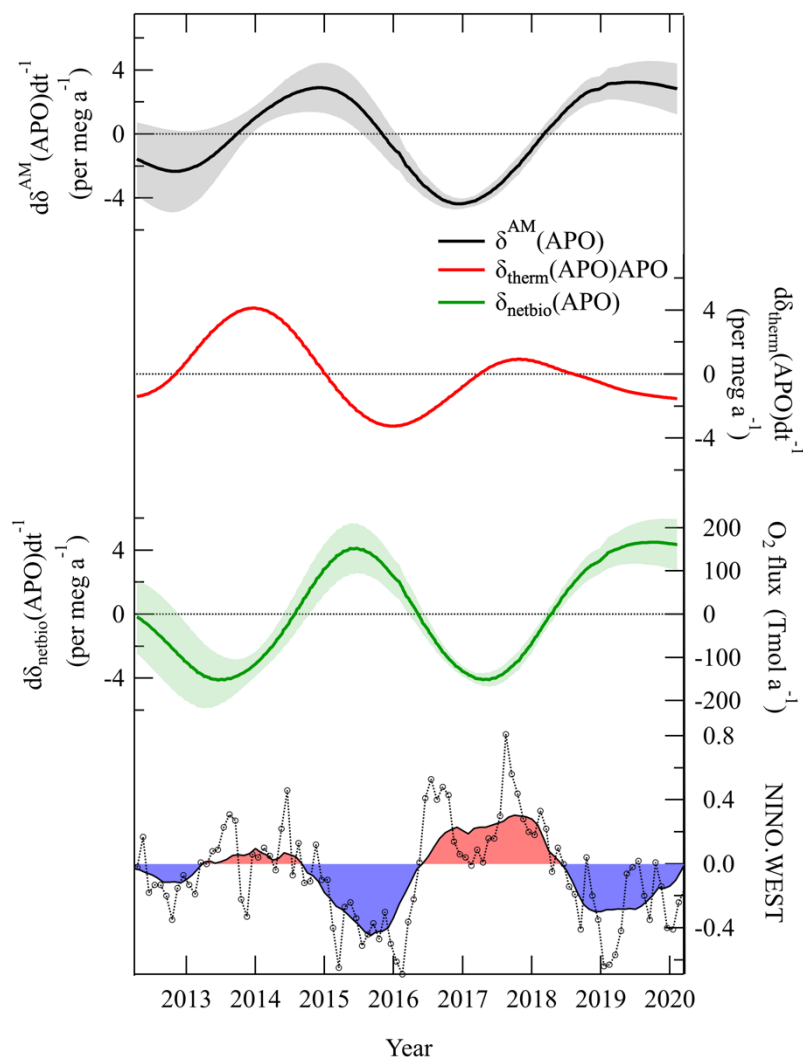
625



630 **Figure 10: Annual change rates of the observed $\delta(\text{APO})$ at each latitude over the western North Pacific (top). The change rates for the APO obtained from the control run of NICAM-TM (middle) and those of $\delta^{\text{AM}}(\text{APO})$ obtained by subtracting the calculated $\delta(\text{APO})$ from the observed $\delta(\text{APO})$ (bottom) are also shown.**



635



640 **Figure 11:** Anomaly in the average annual change rate of $\delta^{\text{AM}}(\text{APO})$ shown at the bottom of Fig. 10 (thick black line). Anomaly in the change rate of APO driven only by the solubility change, expected from the observed surface $\delta(\text{Ar}/\text{N}_2)$ at Tsukuba, Japan ($\delta_{\text{therm}}(\text{APO})$; red line, see text), and that driven by the net marine biospheric activities ($\delta_{\text{netbio}}(\text{APO})$; green line) obtained by subtracting the change rate of $\delta_{\text{therm}}(\text{APO})$ from that of $\delta^{\text{AM}}(\text{APO})$ are shown. Anomaly in the global air-sea O_2 flux corresponding to the change rate of $\delta_{\text{netbio}}(\text{APO})$ is also shown (see text). The time series of the NINO.WEST index (black open circles) and the annual average values of the index (thin black line) are shown at the bottom of the figure.